



**HAL**  
open science

## Seasonal and long-term consequences of esca grapevine disease on stem xylem integrity

Giovanni Bortolami, Elena Farolfi, Eric Badel, Regis Burlett, Herve Cochard, Nathalie Ferrer, Andrew King, Laurent J. Lamarque, Pascal Lecomte, Marie Marchesseau-Marchal, et al.

### ► To cite this version:

Giovanni Bortolami, Elena Farolfi, Eric Badel, Regis Burlett, Herve Cochard, et al.. Seasonal and long-term consequences of esca grapevine disease on stem xylem integrity. *Journal of Experimental Botany*, 2021, 72 (10), pp.3914-3928. 10.1093/jxb/erab117 . hal-03276371

**HAL Id: hal-03276371**

**<https://hal.inrae.fr/hal-03276371v1>**

Submitted on 27 Nov 2024

**HAL** is a multi-disciplinary open access archive for the deposit and dissemination of scientific research documents, whether they are published or not. The documents may come from teaching and research institutions in France or abroad, or from public or private research centers.

L'archive ouverte pluridisciplinaire **HAL**, est destinée au dépôt et à la diffusion de documents scientifiques de niveau recherche, publiés ou non, émanant des établissements d'enseignement et de recherche français ou étrangers, des laboratoires publics ou privés.

# 1 **Seasonal and long-term consequences of esca on grapevine stem xylem** 2 **integrity**

3 **Running title:** Impact of the trunk disease esca on stem hydraulic integrity

4  
5 **Highlight:** Our study reveals that esca can critically affect xylem water movement in grapevine  
6 perennial organs, by the presence of plant-derived tyloses.

7  
8 G. Bortolami<sup>a</sup>, E. Farolfi<sup>a</sup>, E. Badel<sup>b</sup>, R. Burlett<sup>c</sup>, H. Cochard<sup>b</sup>, N. Ferrer<sup>a</sup>, A. King<sup>d</sup>, L.J.  
9 Lamarque<sup>c,e</sup>, P. Lecomte<sup>a</sup>, M. Marchesseau-Marchal<sup>a</sup>, J. Pouzoulet<sup>f</sup>, J.M. Torres-Ruiz<sup>b</sup>, S.  
10 Trueba<sup>c,g</sup>, S. Delzon<sup>c</sup>, G.A. Gambetta<sup>f</sup>, C.E.L. Delmas<sup>a\*</sup>

11  
12 <sup>a</sup>INRAE, BSA, ISVV, SAVE, 33882 Villenave d'Ornon, France

13 <sup>b</sup>Université Clermont-Auvergne, INRAE, PIAF, 63000 Clermont-Ferrand, France

14 <sup>c</sup>Univ. Bordeaux, INRAE, BIOGECO, 33615 Pessac, France

15 <sup>d</sup>Synchrotron SOLEIL, L'Orme des Merisiers, Gif-sur-Yvette, 91192, France

16 <sup>e</sup>Département des Sciences de l'Environnement, Université du Québec à Trois-Rivières, Trois-  
17 Rivières, Québec, G9A 5H7, Canada

18 <sup>f</sup>EGFV, Bordeaux-Sciences Agro, INRAE, Université de Bordeaux, ISVV, 210 chemin de  
19 Leysotte, 33882 Villenave d'Ornon, France

20 <sup>g</sup>School of Forestry and Environmental Studies, Yale University, New Haven, CT 06511, USA

21  
22 \*Author for correspondence

23 Chloé E. L. DELMAS

24 [chloe.delmas@inrae.fr](mailto:chloe.delmas@inrae.fr)

25 ORCID ID: [0000-0003-3568-605X](https://orcid.org/0000-0003-3568-605X)

26

27 **ABSTRACT**

28 Hydraulic failure has been extensively studied during drought-induced plant dieback, but its  
29 role in plant-pathogen interactions is under debate. During esca, a grapevine (*Vitis vinifera*)  
30 disease, symptomatic leaves are prone to irreversible hydraulic dysfunctions but little is known  
31 about the hydraulic integrity of perennial organs over the short- and long-term. We  
32 investigated the effects of esca on stem hydraulic integrity in naturally infected plants within  
33 a single season and across season(s). We coupled direct ( $k_s$ ) and indirect ( $k_{th}$ ) hydraulic  
34 conductivity measurements, and tylose and vascular pathogen detection with in vivo X-ray  
35 microtomography visualizations. We found xylem occlusions (tyloses), and subsequent loss  
36 of stem  $k_s$ , in all of the shoots with severe symptoms (apoplexy) and in more than 60% of the  
37 shoots with moderate symptoms (tiger-stripe), and no tyloses in shoots that were currently  
38 asymptomatic. In vivo stem observations demonstrated that tyloses were observed only when  
39 leaf symptoms appeared, and resulted in more than 50% PLC in 40% of symptomatic stems,  
40 unrelated to symptom age. The impact of esca on xylem integrity was only seasonal and no  
41 long-term impact of disease history was recorded. Our study demonstrated how and to what  
42 extent a vascular disease such as esca, affecting xylem integrity, could amplify plant mortality  
43 by hydraulic failure.

44

45 **Key words:** Esca, hydraulic failure, plant dieback, tyloses, vascular pathogens, *Vitis vinifera*  
46 L., X-ray microCT, xylem anatomy

## 47 INTRODUCTION

48 In agricultural and forest ecosystems, perennial plant dieback causes decreases in plant  
49 productivity and longevity (Aleemullah and Walsh, 1996; Eskalen *et al.*, 2013; Urbez-Torres  
50 *et al.*, 2013; Alvindia and Gallema, 2017). Plant dieback is a complex process where different  
51 biotic and/or abiotic stress factors interact and contribute to leaf and crown wilting and  
52 ultimately plant death (Desprez-Lostau *et al.*, 2006; Anderegg *et al.*, 2013, Cailleret *et al.*,  
53 2017; Bettenfeld *et al.*, 2020). Drought-mediated plant dieback has been extensively studied,  
54 and in this case hydraulic failure has been identified as the primary cause of plant death  
55 (Anderegg *et al.*, 2016). Hydraulic failure results from an interruption of the ascendant water  
56 flow by air embolism or xylem occlusion (Zimmermann, 1979; Tyree and Sperry, 1989).  
57 Vascular pathogens, which infect the xylem network (Yadeta and Thomma, 2013), are also  
58 important drivers of pathogen-mediated plant dieback (Goberville *et al.*, 2016; Pandey *et al.*,  
59 2018; Fallon *et al.*, 2020).

60 Vascular pathogens induce wood necrosis, leaf symptoms, and crown defoliation (Beckmann  
61 and Roberts, 1995; Pearce, 1996). Their biology and toxic metabolite production has been well  
62 studied, in particular using controlled phytotoxicity assays (Andolfi *et al.*, 2011; Akpaninyang  
63 and Opara, 2017). However, the possible role of hydraulic failure during pathogen-mediated  
64 plant dieback has been poorly investigated, and the underlying physiological mechanisms  
65 inducing leaf symptoms are not clear yet (Fradin and Thomma, 2006; McDowell *et al.*, 2008).  
66 Moreover, the long-term impact (over seasons) and relationships between pathogens, leaf  
67 symptom presence, and the hydraulic functioning of the plant are still unknown. During  
68 vascular pathogenesis, both air (Pérez-Donoso *et al.*, 2016) and nongaseous (Sun *et al.*, 2013;  
69 Czemmél *et al.*, 2015, Pouzoulet *et al.*, 2019) embolism have been observed. For example, air  
70 embolism is thought to accelerate pathogen progression during Pierce's disease (Pérez-Donoso  
71 *et al.*, 2016), and nongaseous embolism is associated with occlusion of the xylem conduits by  
72 the plant that could slow the disease process while interfering with xylem water transport (Sun  
73 *et al.*, 2013; Pouzoulet *et al.*, 2019).

74 Xylem occlusion, usually through the production of tyloses and gels, is one of the first plant  
75 defense mechanisms against vascular pathogens (Pearce, 1996). Xylem parenchyma cells  
76 secrete gels and expand into the vessel lumen, forming tyloses, physically blocking pathogen  
77 progression (Zimmermann, 1979). Xylem anatomy plays an important role, both for vascular  
78 pathogen development (Martin *et al.*, 2009; Martín *et al.*, 2013; Venturas *et al.*, 2014;

79 Pouzoulet *et al.*, 2017; 2020) and for tylose formation (Bonsen and Kucera, 1990; De Micco *et*  
80 *al.*, 2016; Pouzoulet *et al.*, 2019). If effective, this occlusion mechanism allows the plant to  
81 compartmentalize the infected zone and to generate new tissue around it (CODIT model,  
82 Pearce, 1996). Because tyloses can potentially interfere with the hydraulic functioning of the  
83 plant, they could exacerbate disease symptoms (Talboys, 1972). Tyloses are usually observed  
84 in close proximity to pathogens, as shown in artificial inoculation studies (Czemmel *et al.*,  
85 2015; Rioux *et al.*, 2018, among others). However, pathogens frequently proliferate in  
86 perennial organs without physically reaching the leaves, thus leaf symptoms are often induced  
87 at a distance (Beckmann and Roberts, 1995). A recent study shows that tyloses can be present  
88 in symptomatic leaves at a distance from the pathogen niches resulting in decreased leaf  
89 hydraulic conductivity (Bortolami *et al.*, 2019).

90 Over the last decades, grapevine (*Vitis vinifera* L.) mortality and yield loss have been reported  
91 in European, American, and South African vineyards due to esca trunk disease (Cloete *et al.*,  
92 2015; Guerin-Dubrana *et al.*, 2019). Esca, a vascular disease caused by the infection of multiple  
93 fungal pathogens, affects mostly mature grapevines (more than seven-years-old), and  
94 symptoms include trunk necrosis and leaf symptoms, consisting of “tiger-stripe” necrosis and  
95 leaf wilting (Lecomte *et al.*, 2012; Claverie *et al.*, 2020), which are not regularly expressed  
96 season-to-season even within individual vines (Guerin-Dubrana *et al.*, 2013; Li *et al.*, 2017).  
97 While the pathogens responsible for esca-induced trunk necrosis have been identified  
98 (Morales-Cruz *et al.*, 2018; Brown *et al.*, 2020), the underlying mechanisms of leaf and fruit  
99 symptoms, and plant death are still poorly understood. Bortolami *et al.* (2019) demonstrated  
100 that the two vascular pathogens related to esca (*Phaeoconiella chlamydospora* and  
101 *Phaeoacremonium minimum*) were never detected in leaves or in stems of the current year, but  
102 always in the trunk (independently from leaf symptom presence). They further showed that  
103 esca symptomatic leaves presented significant losses in hydraulic conductivity due to the  
104 occlusion of the xylem conduits by tyloses. Together, these results reveal that esca impacts leaf  
105 hydraulic functioning, but whether or not there is a corresponding failure in perennial organs,  
106 and the exact timing of this phenomenon, are still unknown. As stems and branches are the  
107 direct connections between the pathogen niche in the trunk and the observed symptoms in the  
108 leaves, the study of stem xylem integrity is crucial in the understanding of esca impact on  
109 grapevine physiology in the current year and across seasons.

110 In this study, we investigated stem xylem integrity in grapevine during esca leaf symptom  
111 formation asking the following questions: (i) Can esca lead to hydraulic failure in perennial  
112 organs? (ii) Does stem hydraulic failure occur prior to or after leaf symptom expression, and  
113 does it depend on xylem anatomy? (iii) Do long-term symptomatic plants present different  
114 xylem anatomy and levels of hydraulic failure from long-term asymptomatic plants? To answer  
115 these questions, we transplanted 28-years-old grapevines (*Vitis vinifera* L. cv Sauvignon blanc)  
116 from the field into pots to transport, manipulate, and study naturally esca-infected vines. We  
117 coupled *in vivo* visualizations of stem xylem functionality (using synchrotron-based X-ray  
118 microcomputed tomography) with stem specific hydraulic conductivity measurements ( $k_s$ ),  
119 theoretical hydraulic conductivity estimates ( $k_{th}$ ), optical observations of vessel occlusions, and  
120 pathogen detection during symptom appearance, while comparing plants with different  
121 symptom history record.

122

## 123 **MATERIALS AND METHODS**

### 124 **Plant material**

125 *Vitis vinifera* cv. Sauvignon blanc grafted onto 101-14 MGt were uprooted in winter 2017,  
126 2018, and 2019 from a vineyard planted in 1992 located at INRAE Bordeaux-Nouvelle  
127 Aquitaine (44°47'24.8"N, 0°34'35.1"W) and transferred into pots. Following plant excavation,  
128 the root system (around 0.125 m<sup>3</sup>) was immersed under water overnight, and powered with  
129 indole-3-butyric acid. The plants were potted in 20l pots in fine clay medium (Klasmann  
130 Deilmann substrate 4:264) and placed on heating plates at 30 °C for two months. Plants were  
131 then moved to a greenhouse, under natural light conditions, and watered with nutritive solutions  
132 (0.1 mM NH<sub>4</sub>H<sub>2</sub>PO<sub>4</sub>, 0.187 mM NH<sub>4</sub>NO<sub>3</sub>, 0.255 mM KNO<sub>3</sub>, 0.025 mM MgSO<sub>4</sub>, 0.002 mM  
133 Fe, and oligo-elements [B, Zn, Mn, Cu, and Mo]) until the end of experiment. Since the  
134 plantation these plants have been trained with a double Guyot system. This training system  
135 requires a permanent main trunk and one cane on each side of the trunk which is left every year  
136 to carry the buds that will produce the stems of the year. During the growing season, the stems  
137 of the current year were trimmed at 1.5-2m, the secondary stems and inflorescences were  
138 removed just after bud-break. Each of these plants has been surveyed each year in the field  
139 since 2012 for esca leaf symptom expression following Lecomte *et al.* (2012), and has been  
140 classified yearly as leaf-symptomatic or asymptomatic. Plants were then classified by their

141 long-term symptomatology record: plants asymptomatic from 2012 to 2018 (pA, previously  
142 asymptomatic), and plants that have expressed symptoms at least once between 2012 and 2018  
143 (pS, previously symptomatic).

#### 144 **Esca symptom notation**

145 The evolution of esca leaf symptoms was surveyed twice a week from June to October 2019  
146 on every plant (n=84, Fig. 1). As presented in Fig. 1A, esca symptoms were scored at the stem  
147 and whole plant scales. The stems of the current year collected for analyses (both hydraulic  
148 measurements or microCT observations) could be noted as: asymptomatic (green leaves and  
149 apparently healthy), pre-symptomatic (leaves presenting yellowing or small yellow spots  
150 between the veins), tiger-stripe (typical pattern of esca leaf symptoms), or apoplectic (leaves  
151 passing from green to wilted in a couple of days). Along the experimentation, entire plants  
152 could be noted as asymptomatic (control) or symptomatic (when at least 25% of the canopy  
153 was presenting tiger-stripe leaf symptoms). At the end of the experiment (week 40, October  
154 2019) each plant was classified as symptomatic or asymptomatic (control). We were then able  
155 to group each stem measured into six different groups (Fig. 1A): one group of stems from  
156 control plants (asymptomatic from June to October) and five groups of stems from  
157 symptomatic plants: two before symptom appearance (asymptomatic and pre-symptomatic  
158 stems); and three after symptom appearance (asymptomatic, tiger-stripe, and apoplectic stems).  
159 To clearly differentiate asymptomatic stems collected from symptomatic plants and  
160 asymptomatic stems collected from asymptomatic plants, we considered plants (and their  
161 stems) that didn't show leaf symptoms during the experiment as control plants (or stems). We  
162 investigated whether symptom expression (final symptom notation in October 2019, see Fig.  
163 1) differed between plants with contrasted long-term symptom history (previously  
164 asymptomatic vs previously symptomatic, Table 1) using a Chi-square test of independence.

165

#### 166 **X-ray microCT observation**

167 Synchrotron-based microCT was used to visualize the content of vessels and their functionality  
168 in esca tiger-stripe and control stems. Three symptomatic plants (presenting tiger-stripe  
169 symptoms for 8, 7, and 3 weeks), and one asymptomatic-control plant were brought to the  
170 PSICHE beamline (King *et al.*, 2016) at SOLEIL synchrotron facility in September 2019.  
171 Stems of the current year (ca. 2 m long) were cut under water and transferred into a solution

172 containing 75mM of contrasting agent iohexol. The iohexol solution absorbs X-rays very  
173 strongly and appears bright white in X-ray scans above the iodine K-edge at 33.2 keV, and,  
174 once it has been taken up by the transpiration stream, the effective functionality of each vessel  
175 can be confirmed (Pratt and Jacobsen, 2018; Bortolami *et al.*, 2019). These stems were moved  
176 and left outdoor to transpire the solution for at least half a day. The stems were then transferred  
177 to the beamline stage and scanned twice in less than 5 minutes using two different energies of  
178 a high-flux ( $3 \times 10^{11}$  photons  $\text{mm}^{-2}$ ) monochromatic X-ray beam: 33.1 keV and 33.3 keV. The  
179 projections were recorded with a sCMOS camera equipped with a 250-mm-thick LuAG  
180 scintillator (Orca Flash, Hamamatsu, Japan). The complete tomographic scan included 1500  
181 projections, and each projection lasted 50 ms. Tomographic reconstructions were performed  
182 using PyHST2 software (Mirone *et al.*, 2014) using the Paganin method (Paganin *et al.*, 2002),  
183 resulting in 32-bit volume reconstructions of 2048 x 2048 x 1024 voxels. The final spatial  
184 resolution was  $2.8769 \mu\text{m}^3 \text{ voxel}^{-1}$ .

### 185 **Image analysis of microCT scans**

186 The contrast agent iohexol allowed us to distinguish in intact scans the effective functionality  
187 of each vessel. In the absence of iohexol, X-ray microCT scans are used to distinguish air-filled  
188 vessels (appearing black, corresponding to native PLC) from sap-filled vessels (appearing  
189 grey). The addition of iohexol in the xylem sap allows to distinguish the functional vessels  
190 (they appear bright white when they transport the sap), from the non-functional ones (i.e.  
191 occluded vessels remaining grey, corresponding to occlusion PLC). We could also observe  
192 partially occluded vessels (i.e. vessels with simultaneous presence of air and occlusions, or sap  
193 and occlusions). This specific case was observed by checking the presence of any occlusion in  
194 at least 200 slices in each volume. Partially occluded vessels were considered as occluded,  
195 some examples are presented in Fig. S1. The equivalent-circle diameter of air-filled, occluded,  
196 and functional (iohexol-filled) vessels was measured on the cross sections from the central slice  
197 of the microCT scanned volume using ImageJ software (Schneider *et al.*, 2012). In the high  
198 energy scans recorded at 33.3 keV X-ray beam, iohexol appears bright white but its contrast  
199 can sometimes impede the clear limit of the vessel lumen. Therefore, all vessel diameters were  
200 recorded on the scan recorded at low energy (33.1 keV X-ray beam), then the distinction of  
201 occluded from iohexol-filled vessels was done on the high energy scan (as done by Bortolami  
202 *et al.* 2019). The theoretical hydraulic conductivity of each vessel ( $k_{vessel}$ ) [ $\text{kg m MPa}^{-1} \text{ s}^{-1}$ ]  
203 was calculated using the Hagen-Poiseuille equation:



204 
$$k_{vessel} = \frac{(\pi \times \varnothing^4 \times \rho)}{(128 \times \eta)}$$

205 Where:  $\varnothing$  is the equivalent circle diameter [m],  $\rho$  the density of water [998.2 kg m<sup>-3</sup> at 20°C],  
206 and  $\eta$  the viscosity of water [1.002 x 10<sup>-9</sup> MPa s at 20°C]. The percentage loss of hydraulic  
207 conductivity given by native air embolism (native PLC) was calculated by the ratio between  
208 the hydraulic conductivity of air-filled vessels and the whole-stem hydraulic conductivity:

209 
$$\text{Native PLC (\%)} = 100 \times \frac{(\sum k_{air-filled\ vessels})}{(\sum k_{all\ vessels})}$$

210 The percentage loss of hydraulic conductivity given by occlusions (occlusion PLC) was  
211 calculated by the ratio between occluded (plus partially occluded) vessels and the whole-stem  
212 hydraulic conductivity:

213 
$$\text{Occlusion PLC (\%)} = 100 \times \frac{(\sum k_{occluded\ vessels} + \sum k_{partially\ occluded\ vessels})}{(\sum k_{all\ vessels})}$$

214

215 The total percentage loss of hydraulic conductivity (total PLC) was obtained by summing  
216 native PLC with occlusion PLC in each sample. As the first ring of xylem vessels (i.e.  
217 protoxylem) was always non-functional (>90% PLC), both in control and tiger-stripe stems, it  
218 was removed from the analysis.

219 We investigated whether native PLC, and occlusion PLC differed between control and esca  
220 tiger-stripe plants, using two independent generalized mixed linear models where plants were  
221 treated as a random effect. Proportional data (ranging from 0 to 1, dividing all PLC values by  
222 100) was analyzed to fit a logit link function and binomial distribution as appropriate.

223

## 224 **Monitoring stem hydraulic properties over time**

225 Xylem integrity was monitored over time by measuring hydraulic properties in stems produced  
226 on the year of the experiment and collected on control and symptomatic plants along the season  
227 and during esca development. Specific hydraulic conductivity ( $k_s$ ) was measured on internodes  
228 sampled in the center of the collected stem by the gravity method (Sperry *et al.*, 1988), and

229 compared to its theoretical analog ( $k_{th}$ ) calculated from xylem anatomical observations on the  
230 same internode or on the one below (see the method described below). When there are observed  
231 differences in  $k_s$  among stems, comparisons with theoretical maximums ( $k_{th}$ ) can show if lower  
232  $k_s$  values result from anatomical differences (i.e. different vessel size distributions) or by  
233 hydraulic failure (in the case of similar vessel size and density). If  $k_s$  varies in unity with  $k_{th}$ ,  
234 differences in  $k_s$  might result from anatomical differences (e.g. smaller  $k_s$  are related to smaller  
235 vessels), otherwise  $k_s$  variations are the consequence of hydraulic failure. Each method to  
236 measure  $k_s$ ,  $k_{th}$ , and to observe tyloses is described below.

237 Sampling started on June 19<sup>th</sup> and finished on September 13<sup>th</sup> 2019 for a total of 10 sampling  
238 dates, 39 stems of the current year from 23 control-asymptomatic plants, and 49 stems of the  
239 current year from 17 symptomatic plants. We randomly sampled control plants and esca  
240 symptomatic plants all along the season through the evolution of esca symptoms, obtaining  
241 measurements from 14 weeks before until 10 weeks after symptom appearance. To explore the  
242 contribution of the experimental design to data analysis, we tested the effect of the year of  
243 uprooting (2018 and 2019), the position of the analyzed internode, and the week of the  
244 measurement (i.e. evolution during the season) on  $k_s$  and  $k_{th}$  in control plants using separate  
245 generalized linear mixed model with normal distributions and the plant treated as a random  
246 variable (Table S1). A significant impact of the year of uproot was found for  $k_s$  and  $k_{th}$  values  
247 in control plants (Table S1). This could have resulted from the more favorable conditions (i.e.  
248 climatic stability and nutrient availability) for the greenhouse grown vines (note that plants  
249 uprooted in 2017 were only esca symptomatic and were not included in this analysis). However,  
250 once  $k_s$  and  $k_{th}$  are plotted together (Fig. S2), all the values lie on the same regression line  
251 without generating outlier values (smaller  $k_s$  values correspond to smaller  $k_{th}$  values  
252 independently of the uprooting year).

### 253 ***Stem specific hydraulic conductivity ( $k_s$ )***

254  $k_s$  measurements were performed on one internode per stem, located in the center of the  
255 collected >1.5m long stem, following Torres-Ruiz *et al.* (2012) gravity method. In the early  
256 morning, each stem was cut at the base under water to avoid air entrance in the stem, maintained  
257 under water and brought to the laboratory. Hydraulic conductivity measurements were always  
258 done before noon, in order to minimize the delay (never more than four hours) from the cut to  
259 the measure. In the laboratory, a representative internode between the 4<sup>th</sup> to the 10<sup>th</sup> internode  
260 from the base (i.e. in the center of the stem) was cut underwater with a clean razor blade, the

261 ends wrapped in tape, and the internode was connected to a pipe system. A flow of 20 mM KCl  
262 solution passed through the sample from a reservoir to a precision electronic balance  
263 (AS220.R2, RADWAG, Radom, PL) recording the weight every 5 seconds using the  
264 WinWedge v3 5.0 software (TAL Technologies, Philadelphia, PA, USA). The solution was  
265 passed through the stem at four increasing pressures (ranging from 0.001 to 0.005 MPa),  
266 controlled by raising the source height. The average flow for each pressure step was determined  
267 after stabilization at a steady-state as the average of 10-15 measures. Hydraulic conductance,  $k$   
268 [ $\text{kg s}^{-1} \text{MPa}^{-1}$ ] was obtained by the slope generated by the flow and the corresponding pressure.  
269 The linear relationship between flow and pressure obtained were always characterized by  
270  $R^2 > 0.97$ . Stem specific hydraulic conductivity,  $k_s$  [ $\text{kg s}^{-1} \text{MPa}^{-1} \text{m}^{-1}$ ], was calculated as follows:

$$271 \quad k_s = \frac{(k \times l)}{A}$$

$$272 \quad A = \left( \left( \frac{d_1}{2} \right)^2 \times \pi \right) - \left( \left( \frac{d_2}{2} \right)^2 \times \pi \right)$$

273 Where:  $k$  is the hydraulic conductance,  $l$  is the length of the sample,  $A$  is the xylem area,  $d_1$  is  
274 the external diameter of the debarked stem, and  $d_2$  is the diameter of the central pith.

### 275 ***Stem theoretical hydraulic conductivity ( $k_{th}$ ), vessel anatomy, and tylose observation***

276 Just before hydraulic conductivity ( $k_s$ ) measurements, the lower internode was stored at 4 °C  
277 in 80% ethanol for analysis of xylem anatomy. When possible, the same internode of  $k_s$   
278 measurements was used for anatomical analysis and  $k_{th}$  estimations, otherwise the stored  
279 internode was used for the following protocol. 50  $\mu\text{m}$  thick slices were obtained using a GSL-  
280 1 microtome (Gärtner *et al.*, 2014). Slices were stained using a 0.5% safranin solution during  
281 5 minutes, and then washed three to four times in ethanol (100%). They were quickly soaked  
282 in xylene and mounted on microscope slides with Permount Mounting Medium (Electron  
283 Microscopy Science, Hatfield, PA, USA). Images were captured with a stereo microscope  
284 SMZ1270 (Nikon, France) mounted with a DS-Fi3 camera (Nikon, France). The theoretical  
285 conductivity of each vessel ( $k_{vessel}$ ) [ $\text{kg m Mpa}^{-1} \text{s}^{-1}$ ] was calculated using the Hagen-Poiseuille  
286 equation as described above.

287 Where  $\varnothing$  is the equivalent circle diameter [m] (measured with ImageJ software),  $\rho$  the density  
288 of water [ $998.2 \text{ kg m}^{-3}$  at 20 °C], and  $\eta$  the viscosity of water [ $1.002 \times 10^{-9} \text{ MPa s}$  at 20 °C].  $k_{th}$

289 of the stem [ $\text{kg s}^{-1} \text{m}^{-1} \text{Mpa}^{-1}$ ] was then calculated by summing every  $k_{vessel}$  in the xylem area  
290 ( $A$ ) [ $\text{m}^2$ ]:

$$291 \quad k_{th} = \frac{\sum k_{vessel}}{A}$$

292 In the entire cross section of each sample, the physical presence (or absence) of tyloses in vessel  
293 lumina was visually assessed.

294 Regarding the statistical analysis, stems were grouped in six different categories following their  
295 esca symptomatology (as presented in Fig. 1A). We investigated whether  $k_s$ ,  $k_{th}$ , and total vessel  
296 density differed among these different categories, and how  $k_s$ ,  $k_{th}$ , and total vessel density  
297 differed between stems with and without tyloses (independently from leaf symptom presence),  
298 using independent mixed linear general models. The symptom / tylose category and the year  
299 of uprooting (since it had a significant impact on  $k_s$  and  $k_{th}$  in control plants, Table S1) were  
300 entered as fixed effects, with the plant treated as a random effect since different stems were  
301 sometimes analyzed from the same plant (88 analyzed stems on 40 different plants). Total  
302 density and densities for each vessel diameter class were log-transformed prior to analysis to  
303 fit normality requirements. For the classes with no vessels (e.g. samples without vessel  
304 diameters above  $160 \mu\text{m}$ ), a minimal density of 0.0001 was assigned prior to log  
305 transformation. We investigated whether the frequency of symptomatic stems presenting  
306 tyloses changed with the symptom age (i.e. weeks between first symptom detection and  $k_s$   
307 measurements on the same plant) with a Chi-square test. The relationships between stem  $k_s$  and  
308  $k_{th}$  were tested using linear regression models. Finally, we investigated whether  $k_s$  and  $k_{th}$  in  
309 control stems differed between plants with different symptom history records using  
310 independent mixed linear general models with the plant treated as a random effect.

311

## 312 **Fungal detection**

313 Detection and quantification of *Phaeoconiella chlamydospora* and *Phaeoacremonium*  
314 *minimum* were performed using qPCR in a subsample of stems of the current year ( $n = 28$ ) and  
315 perennial trunks ( $n = 20$  plants) from the same symptomatic and control plants used for  
316 hydraulic and anatomical measurements. All along the season, basal internodes, from the same  
317 stems sampled for  $k_s$  and  $k_{th}$  measurements, were directly placed in liquid nitrogen and stored

318 at -80 °C. At the end of the experiment, a subset of plants was cut at the base for trunk sampling.  
319 A 2 cm high section was cut with a sterilized hand saw. The bark was removed and the different  
320 tissues of each section (necrotic and apparently healthy wood) were separately collected using  
321 ethyl alcohol-sterilized shears in a sterile environment, and immediately placed in liquid  
322 nitrogen. All samples were ground in liquid nitrogen using a tissue lyser (Tissuelyser II,  
323 Qiagen, Germantown, MD, USA). DNA was extracted from 60mg of ground tissue using the  
324 Invisorb Spin Plant Mini Kit (Invitek GmbH, Berlin, Germany) according to the manufacturer's  
325 instructions. . Detection and quantification of *P. chlamydospora* and *P. minimum* (previously  
326 named *P. aleophilum*) DNA by qPCR (SYBR Green assays) was conducted using the primer  
327 sets PchQF (5'-CTCTGGTGTGTAAGTTCAATCGACTC-3')/PchQR (5'-  
328 CCATTGTAGCTGTTCCAGATCAG-3') and PalQF(5'-  
329 CCGGTGGGGTTTTTACGTCTACAG-3')/ PalQR(5'-  
330 CGTCATCCAAGATGCCGAATAAAG-3') (Pouzoulet *et al.* 2013). The qPCR reactions  
331 proceeded in a final volume of 25 µl, and the reaction mixtures containing 2 µL of DNA  
332 template, 12.5 µl of 2X SYBRGreen Quantitect Master Mix (Qiagen, Venlo, Netherlands), and  
333 each primer at a final concentration of 0.4 µM. Experiments were conducted with a Mx3005P  
334 Real-Time PCR cycler using MxPro qPCR software (Agilent Technologies). The cycling  
335 program, as described in Pouzoulet *et al.* (2017), consisted of an initial denaturation step at  
336 95°C for 15 min, and 40 cycles of 15 s at 95°C (for denaturation) followed by 45 s at 62°C (for  
337 both annealing and extension). A melting analysis of 40 min from 60 to 95° was performed to  
338 verify reaction's specificity and the absence of byproducts. Preparation and use of standard  
339 solutions for the absolute quantification of fungal DNA was realized following Pouzoulet *et al.*  
340 (2013) using ten-fold dilutions of fungal DNA extracts obtained from axenic cultures. Reaction  
341 efficiencies ranging from 90% and 95% with an  $R^2 > 0.99$  (n=15) were obtained for both  
342 PchQF/R and PalQF/R primer sets. The average amount of DNA was determined based on  
343 three technical replicates (standards and plates) with a detection threshold superior to 95% (i.e.  
344 at least three positive amplification out of three replicates) or otherwise discarded (i.e. pathogen  
345 DNA was considered absent). Pathogen DNA quantity (average value of three technical  
346 replicates, fg/µl) was normalized by the amount of total DNA (ng/µl), measured using a Qubit  
347 fluorometer. The results from each trunk sample (i.e. necrotic or apparently healthy wood) were  
348 averaged together in order to obtain one quantification per plant. We investigated whether the  
349 amount of fungal DNA (both for *P. chlamydospora* and for *P. minimum*) in trunks differed  
350 between symptomatic and control plants, and between control plants with different symptom

351 history records, using generalized linear mixed model with a poisson distribution and a log  
352 likelihood function.

353

### 354 **Statistical analysis**

355 All data management and statistical tests were done in SAS software (SAS 9.4; SAS Institute).  
356 We used PROC GLIMMIX for generalized linear mixed models, PROC GLM for generalized  
357 linear models, PROC REG for regression analyses and PROC FREQ for frequency analyses  
358 (Chi-square test of independence). The normality of the response variables was tested using a  
359 Kolmogorov-Smirnov test (PROC UNIVARIATE) prior to analyses. Data were log-  
360 transformed (total density) or appropriate distributions (binomial, poisson) were fitted when  
361 appropriate.

362

## 363 **RESULTS**

### 364 **Esca leaf symptom expression within and across seasons**

365 Esca leaf symptoms were recorded in 20 out of the 58 plants followed in this study (35%, Fig.  
366 1, Table 1). The number of symptomatic plants increased gradually with time, from the first  
367 symptom appearance in early June to the last in late September (Fig. 1). There was no effect of  
368 the plant history (previously asymptomatic pA, or previously symptomatic pS) on 2019  
369 symptom expression ( $n=58$ ,  $X^2=0.27$ ,  $P=0.60$ ). On 20 pA plants, six (30%) expressed leaf  
370 symptoms in 2019 (Table 1). On 38 pS plants, fourteen (37%) showed symptoms in 2019  
371 (Table 1). However, pS plants expressed symptoms from June to the end of September, while  
372 pA plants showed leaf symptoms only in September.

373

### 374 ***In vivo* observations of esca symptomatic stems**

375 Xylem vessels of control and tiger-stripe stems were observed using three dimensional X-ray  
376 microCT scans in iohexol-fed samples (Fig. 2, 3, Table S2). As shown in Fig. 2, functional and  
377 non-functional vessels can be discriminated through the use of iohexol (functional vessels  
378 appear bright white, non functional vessels appear either black if air-filled or grey if occluded).

379 We observed almost totally functional stems in all asymptomatic stems (<20% total PLC, Fig.  
380 2A-C), and 40% of tiger-stripe stems (e.g. Fig. 2D-G). Higher levels of PLC (>20% total PLC,  
381 Fig H-M) were observed in the remaining tiger-stripe stems, with 40% of tiger-stripe stems  
382 exhibiting over 50% total PLC (Fig. 2J-M). When the two components of PLC were  
383 disentangled, we observed that the level of native PLC remained low both in control ( $6.5 \pm$   
384  $2.6\%$ ) and in tiger-stripe ( $12.2 \pm 2.9\%$ ) stems (Fig. 3A). Occlusion PLC values were virtually  
385 zero in control stems ( $0.7 \pm 0.02\%$ ) while in tiger-stripe stems the mean occlusion PLC values  
386 was  $27.5 \pm 8.2\%$  (Fig. 3B). Nevertheless, the variability of occlusion PLC across tiger-stripe  
387 stems was very high, the values ranging from 0.3% to 72.9% (Fig. 2D-M, and 3B), and  
388 occlusion PLC was not correlated to symptom age ( $n=10$ ,  $F_{2,7}=0.19$ ,  $P=0.83$ ). Consequently,  
389 no statistical differences in native or occlusion PLC were found between control and tiger-  
390 stripe stems (Fig. 3). When higher occlusion PLC was measured (Fig. 2H-M), occluded vessels  
391 could be organized either on one side of the stem (Fig 2J-L) or randomly distributed across the  
392 section (Fig 2H, 2I, 2M). In 90% of symptomatic stems, we observed that the most external  
393 vessels were functional. Occlusions were present equally in all vessel diameter classes (Fig.  
394 S3).

395

### 396 **Tylose development, stem specific ( $k_s$ ) and theoretical ( $k_{th}$ ) hydraulic conductivity during** 397 **esca leaf symptom formation**

398 Tyloses were identified in the xylem vessels of certain tiger-stripe stems and throughout the  
399 temporal development of esca leaf symptoms, from the appearance of symptoms to 11 weeks  
400 after. All apoplectic stems and 62.5% (15 of 24 analyzed stems) of esca tiger-stripe stems  
401 presented tyloses, while all other stems (control, asymptomatic or pre-symptomatic) did not  
402 contain these occlusions, even until one week before symptom development. In esca tiger-  
403 stripe stems, tyloses were not related to specific plants, or to symptom age (i.e. on the same  
404 plant at the same moment, different symptomatic stems could present tyloses, or not,  $n=24$ ,  
405  $\chi^2=7.47$ ,  $P=0.38$ ).

406 Overall, no significant impact of esca symptoms was observed on  $k_s$  (Fig. 4A), even if tiger-  
407 stripe stems were divided between those with and without tyloses. Control stems presented a  
408 mean ( $\pm$  SE)  $k_s$  of  $24.97 \pm 1.72 \text{ kg s}^{-1} \text{ MPa}^{-1} \text{ m}^{-1}$ ; all the stems without tyloses measured on  
409 symptomatic plants showed the same range of values as control stems (Fig 4A, Table 2): 26.04

410  $\pm 4.71$  for asymptomatic before symptoms appearance,  $30.32 \pm 4.26$  for pre-symptomatic  
411 stems,  $19.80 \pm 5.18$  for asymptomatic stems after symptom appearance on the plant, and  $21.29$   
412  $\pm 5.40$  for tiger-stripe stems without tyloses. Stems with tyloses (tiger-stripe and apoplectic  
413 stems) presented the lowest average  $k_s$  values ( $11.27 \pm 2.86$  and  $2.47 \pm 1.45$   $\text{kg s}^{-1} \text{MPa}^{-1} \text{m}^{-1}$   
414 for tiger-stripe and apoplectic, respectively). Regarding  $k_{th}$ , no significant impact of esca  
415 symptoms was found (Fig. 4C, Table 2), all the values were in the same range, with average  
416 values ranging from 70.44 (for tiger-stripe stems with tyloses) to 87.88 (for pre-symptomatic  
417 stems)  $\text{kg s}^{-1} \text{MPa}^{-1} \text{m}^{-1}$ .

418 In order to further investigate the impact of esca on stem hydraulics, we explored the  
419 relationship between individual stem  $k_s$  and  $k_{th}$  in each symptom category (Fig. 4B, S4, Table  
420 2). Significant relationships were found between  $k_s$  and  $k_{th}$  in all groups except in asymptomatic  
421 stems after symptom appearance and symptomatic stems with the physical presence of tyloses  
422 (Fig. S4, Table 2). The slopes of regression curves between  $k_s$  and  $k_{th}$  did not vary among  
423 groups in the absence of tyloses (slope values ranged between 0.3 and 0.4, Table 2) while it  
424 was close to 0 in the presence of tyloses (0.17 for tiger-stripe and 0.04 for apoplectic stems).  
425 When  $k_s$  and  $k_{th}$  are compared in the presence or absence of tyloses, we observed that  $k_s$  was  
426 significantly lower when tyloses were present ( $9.81 \pm 2.51$   $\text{kg s}^{-1} \text{MPa}^{-1} \text{m}^{-1}$  in the presence of  
427 tyloses vs  $25.06 \pm 1.46$   $\text{kg s}^{-1} \text{MPa}^{-1} \text{m}^{-1}$  in the absence of tyloses, Table 2,  $n=88$ ,  $F_{1,49}=7.11$ ,  
428  $P=0.01$ ) while  $k_{th}$  did not significantly differ. Stems without tyloses presented a strong  
429 correlation between  $k_s$  and  $k_{th}$ , while in the presence of tyloses this relationship was not  
430 significant (Table 2, Fig. 4B).

431 Total vessel density did not significantly differ between stem symptomatology (comparing all  
432 the seven categories presented in Table 2), even when vessel density was partitioned by vessel  
433 diameter classes (Fig. 4D).

434 Finally, we tested the impact of disease history (comparing pA and pS plants) on the hydraulic  
435 conductivity and xylem anatomy in control plants. There were no differences between long-  
436 term symptomatic (pS) and long-term asymptomatic (pA) plants in stem  $k_s$ , stem  $k_{th}$ , or total  
437 vessel density (Table 3).

438

439 **Fungal detection**



440 The two vascular pathogens associated with esca (*Phaeoconiella chlamydospora* and  
441 *Phaeoacremonium minimum*) were never detected in stems of the current year while they were  
442 systematically detected in the perennial trunk of both control and symptomatic plants (Table  
443 4). In trunks, a significantly higher quantity of fungal DNA was detected in tiger-stripe  
444 symptomatic plants than in controls (Table 4). We found 2.14- and 1.64-fold more of *P.*  
445 *chlamydospora* and *P. minimum* DNA in symptomatic trunks relative to controls. In control  
446 plants, different symptom history records impacted the quantity of fungal DNA detected by  
447 qPCR, for *Phaeoconiella chlamydospora*, and for *Phaeoacremonium minimum*. We found  
448 1.65- and 2.84-fold more *P. chlamydospora* and *P. minimum* DNA in previously symptomatic  
449 trunks relative to previously asymptomatic trunks (Table 3).

450

## 451 **DISCUSSION**

452 Our results regarding the impact of esca on stem xylem integrity show that the presence of  
453 plant-derived tyloses induced hydraulic failure in 60% of symptomatic stems of the current  
454 year. Tyloses were only observed in symptomatic stems, and resulted in more than 50% PLC  
455 in 40% of the stems, unrelated to symptom age. We demonstrated that the presence of leaf  
456 symptoms during previous seasons had no impact on the likelihood of symptom appearance in  
457 the current year, or on stem hydraulic conductivity and xylem anatomy. Vascular fungi were  
458 never detected in the same organs as the tyloses (stems of the current year), and although they  
459 were present in trunks of both tiger-stripe and control plants, tiger-stripe plants showed higher  
460 quantities of fungal DNA. Among control plants that did not express symptoms in the year of  
461 the study, we found higher quantities of fungal DNA in trunks of those plants with a long-term  
462 history of symptom formation. Albeit xylem occlusions were not observed in the totality of  
463 tiger-stripe stems, they could amplify yield loss plant mortality, especially in the context of  
464 climate change as they impair water transport in a majority of symptomatic stems.

465

### 466 ***In vivo* xylem integrity observations and hydraulic vulnerability segmentation**

467 Using direct X-ray microCT imaging in esca symptomatic stems, we found that hydraulic  
468 conductivity loss was almost entirely associated with the presence of tyloses. Different studies  
469 have investigated the link between vascular pathogen development and hydraulic conductivity

470 in stems (Collins *et al.*, 2009; Lachenbruch and Zhao, 2019; Mensah *et al.*, 2020). During biotic  
471 stresses, air embolisms have been shown to decrease hydraulic conductivity during bacterial  
472 leaf scorch disease (McElrone *et al.*, 2003; 2008), Pierce's disease (Pérez-Donoso *et al.*, 2016),  
473 and Pine wilt disease (Yazaki *et al.*, 2018). In the case of fungal wilt diseases, the hydraulic  
474 conductivity loss was associated with nongaseous embolism (i.e. tyloses) at the point of  
475 pathogen inoculation (Guerard *et al.*, 2000; Sallé *et al.*, 2008; Beier *et al.*, 2017; Mensah *et al.*,  
476 2020), or with canker presence in naturally infected stems (Lachenbruch and Zhao, 2019).

477 Using iohexol we were able to visually observe the exact spatial organization of functional  
478 vessels. Interestingly, in some symptomatic samples we found functional vessels surrounding  
479 the non-functional xylem (Fig. 2J-L), suggesting that the plant was able to preserve the more  
480 external vessels from occlusions or to form new functional vessels after the loss of  
481 conductivity. Moreover, the sectoriality of the occlusions observed in Fig. 2J-L was  
482 reminiscent of the sectoriality observed in the distributions of trunk necrosis, especially on the  
483 brown stripe necrosis appearing along the vasculature (Lecomte *et al.*, 2012).

484 Comparing these results with our precedent study using the same technique in leaves, we  
485 showed that esca symptomatic leaves presented higher levels of occlusion PLC ( $61 \pm 7\%$  in  
486 midribs, and  $54 \pm 9\%$  in petioles, data from Bortolami *et al.*, 2019) compared to stems ( $27 \pm 8$   
487 %, occlusion PLC), suggesting hydraulic vulnerability segmentation (although PLC in leaves  
488 and stems were measured in different plants and years). The hydraulic segmentation theory  
489 relies on the fact that annual organs (i.e. leaves) are more vulnerable than perennial organs (i.e.  
490 stems) to drought induced air embolism (Tyree and Ewers, 1991). Grapevine is well known for  
491 exhibiting strong hydraulic vulnerability segmentation (Charrier *et al.*, 2016; Hochberg *et al.*,  
492 2016; 2017). This is thought to be adaptive, where the higher vulnerability in leaves and  
493 petioles favors embolism formation and leaf shedding prior to embolism formation in stems,  
494 thus protecting the perennial organs. Our observations during esca pathogenesis demonstrate  
495 that, analogous to the hydraulic vulnerability segmentation theory, leaves appear more  
496 vulnerable to the formation of nongaseous embolism as well, which could mitigate the risk of  
497 hydraulic failure in perennial organs. From another perspective, the difference may not be a  
498 direct effect of the specific organ's vulnerability to nongaseous embolism, but a consequence  
499 of a difference in the accumulation of putative toxins and/or elicitors. Indeed, we confirmed  
500 here that esca leaf symptoms occur at a distance from the pathogen niche because vascular  
501 pathogens were never detected in stems of the current year, suggesting that the plant may

502 transport a signal (i.e. toxins or elicitors) from the infected trunk up to the leaves. If the signal  
503 accumulates in leaves in a higher amount than it does in the stems (water potentials are more  
504 negative in leaves compared to stems), and stimulates occlusion formation, stems would then  
505 be secondarily affected.

506

## 507 **Hydraulic conductivity, tyloses, and vessel anatomy**

508 Tyloses could have different impacts, both positive and negative, during wilt disease  
509 pathogenesis: (i) tyloses contribute to pathogen resistance as they aim to seal off vessel lumens  
510 and impede pathogens spread throughout the host (CODIT model, Shigo, 1984). This is the  
511 case regarding the susceptibility of different species or varieties to specific pathogens (Jacobi  
512 and MacDonald, 1980; Ouellette *et al.*, 1999; Clériveret *et al.*, 2000; Et-Touil *et al.*, 2005;  
513 Venturas *et al.*, 2014; Park and Juzwik 2014; Rioux *et al.*, 2018), in particular to *Phaeomonilla*  
514 *chlamydospora*, one of the pathogen associated with esca (Pouzoulet *et al.*, 2017; 2020). (ii) In  
515 other studies, it has been shown that tyloses can exacerbate symptoms (Talboys, 1972): they  
516 cause a reduction in stem hydraulic conductivity, sometimes associated with a reduction in  
517 stomatal conductance in leaves and, in the most severe cases, wilting (Parke *et al.*, 2007; Beier  
518 *et al.*, 2017; Lachenbruch and Zhao, 2019, Mensah *et al.*, 2020 during fungi development; Sun  
519 *et al.*, 2013; Deyett *et al.*, 2019 during Pierce's disease). Our results suggest that during esca  
520 tyloses might lead to symptom exacerbation. Esca has also been suggested to lead to a general  
521 reduction in xylem water transport and stomatal conductance (Ouadi *et al.*, 2019), and tyloses  
522 could be a major contributor to these phenomena as during winter senescence (Salleo *et al.*,  
523 2002; Sun *et al.*, 2008). However, when symptomatic stems have no tyloses (~37% of the stems  
524 with tiger-stripe symptoms), esca leaf symptom formation seems to arise from within the leaf  
525 itself, and may not result from upstream hydraulic failure. Although tyloses were never  
526 detected in asymptomatic stems prior to the onset of leaf symptoms, the time sequence of tylose  
527 and leaf symptom development has still to be determined. Since both the microCT and  
528 anatomical observations visualize relatively narrow regions of the stems, tylose presence could  
529 have been underestimated (i.e. if there was additional tylose development up or downstream of  
530 the stem sections visualized). However, it should be pointed out that if significant  
531 underestimation were present we would expect some loss of conductivity even in internode  
532 sections from which we observed no tyloses in the sampled cross sections. At least when

533 considering a single internode our direct hydraulic conductivity measurements do not support  
534 the hypothesis that tyloses were underestimated (Fig. 4B).

535 Xylem is the battleground between vascular pathogens and the plant's defense response  
536 (Yadeta and Thomma, 2013). Even if xylem vessel anatomy is less investigated, it could have  
537 a crucial role in plant resistance and response to vascular pathogens. For example, during Dutch  
538 elm wilt disease (due to *Ophiostoma spp.*) the most sensitive species and varieties present wider  
539 xylem vessels (Elgersma, 1970; McNabb *et al.*, 1970; Solla and Gil 2002; Pita *et al.*, 2018).  
540 Smaller vessels could occlude faster, sustaining a more efficient pathogen restriction (Venturas  
541 *et al.*, 2014). Our results on xylem vessel anatomy suggest that stems with tyloses tend to  
542 present higher densities of small vessels, even if we did not observe any differences in total  $k_{th}$   
543 values and microCT scans showed that occlusions appear randomly in every vessel size class  
544 (Fig. S3). It could be possible that tylose formation might be interfering with stem water  
545 relations reducing the carbohydrates available for plant growth, producing smaller vessels in  
546 stems of symptomatic plants. In contrast, artificial inoculations showed that xylem vessel  
547 diameter had a strong impact on esca-related vascular pathogen development (Pouzoulet *et al.*,  
548 2017; 2020), and in the kinetic of vessel occlusion in grapevine stems (Pouzoulet *et al.*, 2019).  
549 The relationships between esca leaf symptoms, xylem anatomy, and tylose presence should be  
550 studied in detail in trunks, where vascular pathogens are present, and among different grapevine  
551 varieties and rootstocks as they are known to show different susceptibility to symptom  
552 expression.

553

#### 554 **Long-term consequences of esca on leaf symptom expression and stem hydraulic integrity**

555 In field surveys, esca leaf symptoms are often randomly distributed spatially throughout  
556 vineyards and are not consistent from season to season in individual vines (Mugnai *et al.*, 1999;  
557 Surico *et al.*, 2000; Marchi *et al.*, 2006; Guerin-Dubrana *et al.*, 2013; Li *et al.*, 2017). However,  
558 esca-related vine death is strongly related to leaf symptoms as death is usually observed  
559 following a year with symptom expression (Guerin-Dubrana *et al.*, 2013). In agreement with  
560 these field studies, we observed similar percentages of symptomatic plants between those that  
561 had already expressed esca symptoms in the past (from one to seven consecutive years, pS  
562 plants), and those that had never expressed symptoms over the past seven years (pA plants).  
563 However, we also found that pS plants expressed symptoms earlier in the season than pA

564 plants, suggesting that symptoms might require more time to develop in pA plants. We did not  
565 find any significant differences in  $k_s$  and  $k_{th}$  values between plants with contrasted long-term  
566 symptom history. This result suggests that esca leaf symptoms may have xylem anatomical  
567 consequences within the year of expression by the production of tyloses, but not across seasons.  
568 Moreover, we showed that DNA pathogen amount (*Phaeoacremonium minimum* and  
569 *Phaeomoniella chlamydospora*) depends on the symptom expression in the season of sampling,  
570 and on the long-term symptom history. Altogether, these results suggest that a higher amount  
571 of vascular fungi in the trunk represents a higher risk in reproducing leaf symptoms, and  
572 consequently, a higher risk of plant death.

573

#### 574 **Hydraulic failure and esca leaf symptom pathogenesis**

575 Our results showed that, even if esca-related stem occlusion was extremely variable, 40% of  
576 the microCT analyzed stems presented a total PLC greater than 50%. Under drought conditions  
577 alone, studies suggest that grapevines are not able to recover in the current season from PLC  
578 greater than 50% in stems (Charrier *et al.*, 2018). Thus, to what extent these levels of esca-  
579 induced hydraulic failure compromise future vine performance, and/or increase the likelihood  
580 of developing esca leaf symptoms in the future remains an open question.

581 We showed that, similarly to visual leaf symptoms, tyloses in stems were generated at a  
582 distance from the pathogen niche in the trunk. Comparing our results with Bortolami *et al.*  
583 (2019), we show that the PLC due to the occlusions (hydraulic failure) observed using microCT  
584 in leaves was on average twice higher than the PLC observed in stems in the present work. We  
585 could hypothesize that, following pathogen activities in the trunk, a signal passing through the  
586 xylem network and stimulating tyloses, first accumulates in leaves and then affects the stems.  
587 However, the exact signal and action remain unknown, as we showed that the presence of  
588 tyloses depended upon given symptomatic stems rather than symptomatic plants (i.e. two stems  
589 in the same plant, with same tiger-stripe symptoms, sampled at the same moment, could or  
590 could not present tyloses).

591 We showed that there were no differences in symptom expression, nor in the stem hydraulic  
592 properties, regarding the long-term symptom history. We can conclude that the processes that  
593 generate tiger-stripe symptoms are largely restricted to the current year of the symptom  
594 expression. However, in plants expressing symptoms for the first time according to our disease

595 record, these processes could require more time, as they showed symptoms only late in the  
596 season. The presence of occlusion, leading to hydraulic failure in stems, could exacerbate leaf  
597 symptom expression in the following seasons, possibly contributing to death. We could  
598 speculate that a stem expressing extensive hydraulic failure could be more prone to express  
599 symptoms in the following year or, in the worst cases, to die. If the level of hydraulic failure  
600 could affect the stem mortality in the following year, the choice of stems with a complete  
601 absence of failure during the winter pruning could reduce the impact of esca in vineyards. The  
602 pruning practices are known to impact the course of infection and leaf symptom development  
603 and it has been shown that trunk renewal could be an effective management practice to prevent  
604 grapevine trunk diseases in the vineyard (Travadon *et al.* 2016, Kaplan *et al.* 2016, Gramaje *et*  
605 *al.* 2018). In addition, the presence of occlusions could also amplify plant susceptibility to  
606 drought-induced hydraulic failure, enhancing the risk of plant mortality in the field as  
607 suggested by McDowell *et al.* (2008). It could be speculated that a decrease in soil water  
608 potential or a high evaporative demand, concomitant to esca-induced hydraulic failure, could  
609 embolize the remaining functional xylem vessels stopping the water flow and desiccating plant  
610 tissues (this could be the case in apoplectic plants for example). In perspective, future studies  
611 should investigate the link between pathogen activities and occlusion development, especially  
612 in trunks, and the subsequent hydraulic failure consequences on whole plant physiology.

### 613 SUPPORTING INFORMATION

614 The following Supporting Information is available for this article:

615 **Fig. S1.** Two-dimensional reconstruction of longitudinal cross sections from X-ray microCT  
616 volumes of grapevine stems.

617 **Fig. S2.** Relationship between  $k_s$  and  $k_{th}$  in control plants.

618 **Fig. S3.** Vessel density and percentage of occluded vessels in tiger-stripe stems for different  
619 vessel diameter classes.

620 **Fig. S4.** Relationships between  $k_s$  and  $k_{th}$  in each stem symptom category.

621 **Table S1.** Effect of year of uprooting, internode analyzed, and sampling date on  $k_s$  and  $k_{th}$  in  
622 control stems.

623 **Table S2.** Calculated theoretical hydraulic conductivity ( $k_{th}$  %), and hydraulic conductivity loss  
624 (PLC %) from X-ray microCT volumes of intact grapevine stems.

625

626

627 **DATA AVAILABILITY STATEMENT**

628 Raw datasets are available in the INRAE dataverse: Bortolami, Giovanni; Farolfi, Elena; Badel,  
629 Eric; Burlett, Regis; Cochard, Herve; Ferrer, Nathalie; King, Andrew; Lamarque, Laurent J.;  
630 Lecomte, pascal; Marchesseau-Marchal, Marie; Pouzoulet, Jerome; Torres-Ruiz, Jose M.;  
631 Trueba, Santiago; Delzon, Sylvain; Gambetta, Gregory A.; Delmas, Chloe E.L., 2021, "Raw  
632 data for the paper "Seasonal and long-term consequences of esca on grapevine stem xylem  
633 integrity"", <https://doi.org/10.15454/U9KJEW>, Portail Data INRAE, V1.

634

635 **ACKNOWLEDGMENTS**

636 We thank the experimental teams of UMR SAVE and UMR EGFV (Bord'O platform, INRAE,  
637 Bordeaux, France) and the SOLEIL synchrotron facility (beamline PSICHE) for providing the  
638 materials and logistics. Specifically, we thank Jérôme Jolivet and Sebastien Gambier (UMR  
639 SAVE) for providing technical knowledge and support for plant transplantation and  
640 maintenance. This work was supported by the French Ministry of Agriculture, Agrifood, and  
641 Forestry (FranceAgriMer and CNIV) within the PHYSIOPATH project (program Plan  
642 National Déperissement du Vignoble, 22001150-1506) awarded to C.E.L.D., and program  
643 Investments for the Future (ANR-10-EQPX-16, XYLOFOREST).

644

645

646 **AUTHOR CONTRIBUTIONS**

647 C.E.L.D., G.A.G., G.B., and S.D. designed the experiments;  
648 E.F., G.A.G., S.D., E.B., R.B., H.C., A.K., L.J.L., J.M.T.-R., S.T. participated in synchrotron  
649 campaigns;  
650 G.B., C.E.L.D., E.F., and N.F. conducted the esca symptom notations;  
651 G.B., M.M.-M., and N.F. conducted the histological observations;  
652 E.F. conducted the hydraulic conductivity measurements and participated to data analyses;  
653 N.F., and J.P., conducted the pathogen detection;  
654 G.B. analyzed the microCT, optical images, and analyzed the data;  
655 P.L. provided data on disease history of the plants;  
656 G.B., C.E.L.D., and G.A.G. wrote the article;  
657 all authors edited and agreed on the last version of the article

658

## REFERENCES

**Akpaninyang FE, Opara EU.** 2017. The Influence of Toxins in Disease Symptom Initiation in Plants: A Review. *Journal of Agriculture and Sustainability* 10, 29-52.

**Aleemullah M., Walsh K.** 1996. Australian papaya dieback: Evidence against the calcium deficiency hypothesis and observations on the significance of laticifer autofluorescence. *Australian Journal of Agricultural Research* 47, 371-385.

**Alvindia DG, Gallema FLM.** 2017. *Lasiodiplodia theobromae* causes vascular streak dieback (VSD)-like symptoms of cacao in Davao Region, Philippines. *Australasian Plant Disease Notes* 12, 54.

**Anderegg WRL, Kane JM, Anderegg LDL.** 2013. Consequences of widespread tree mortality triggered by drought and temperature stress. *Nature Climate Change* 3, 30-36.

**Anderegg WRL, Klein T, Bartlett M, Sack L, Pellegrini AFA, Choat B, Jansen S.** 2016. Meta-analysis reveals that hydraulic traits explain cross-species patterns of drought-induced tree mortality across the globe. *Proceedings of the National Academy of Sciences* 113, 5024-5029.

**Andolfi A, Mugnai L, Luque J, Surico G, Cimmino A, Evidente A.** 2011. Phytotoxins Produced by Fungi Associated with Grapevine Trunk Diseases. *Toxins* 3, 1569-1605.

**Beckman CH, Roberts EM.** 1995. On the Nature and Genetic Basis for Resistance and Tolerance to Fungal Wilt Diseases of Plants. *Advances in Botanical Research* 21, 35-77.

**Beier GL, Held BW, Giblin CP, Cavender-Bares J, Blanchette RA.** 2017. American elm cultivars: Variation in compartmentalization of infection by *Ophiostoma novo-ulmi* and its effects on hydraulic conductivity. *Forest Pathology* 47, 1-11.

**Bettenfeld P, Fontaine F, Trouvelot S, Fernandez O, Courty P-E.** 2020. Woody Plant Declines. What's Wrong with the Microbiome? *Trends in Plant Science* 25, 381-394.

**Bonsen KJM, Kučera LJ.** (1990). Vessel Occlusions in Plants: Morphological, Functional and Evolutionary Aspects. *IAWA Journal* 11, 393-399.



**Bortolami G, Gambetta GA, Delzon S, et al.** (2019). Exploring the Hydraulic Failure Hypothesis of Esca Leaf Symptom Formation. *Plant Physiology* 181, 1163-1174.

**Brown AA, Lawrence DP, Baumgartner K.** 2020. Role of basidiomycete fungi in the grapevine trunk disease esca. *Plant Pathology* 69, 205-220.

**Cailleret M, Jansen S, Robert EMR, et al.** 2017. A synthesis of radial growth patterns preceding tree mortality. *Global Change Biology* 23, 1675-1690.

**Charrier G, Delzon S, Domec J-C, et al.** 2018. Drought will not leave your glass empty: Low risk of hydraulic failure revealed by long-term drought observations in world's top wine regions. *Science Advances* 4, 1-9.

**Charrier G, Torres-Ruiz JM, Badel E, et al.** 2016. Evidence for Hydraulic Vulnerability Segmentation and Lack of Xylem Refilling under Tension. *Plant Physiology* 172, 1657-1668.

**Claverie M, Notaro M, Fontaine F, Wery J.** 2020. Current knowledge on Grapevine Trunk Diseases with complex etiology : A systemic approach. *Phytopathologia Mediterranea* 59, 29-53.

**Clériveret A, Déon V, Alami I, Lopez F, Geiger J-P, Nicole M.** 2000. Tyloses and gels associated with cellulose accumulation in vessels are responses of plane tree seedlings (*Platanus × acerifolia*) to the vascular fungus *Ceratocystis fimbriata* f. *Sp platani*. *Trees* 15, 25-31.

**Cloete M, Mostert L, Fischer M, Halleen F.** 2015. Pathogenicity of South African Hymenochaetales taxa isolated from esca-infected grapevines. *Phytopathologia Mediterranea* 54, 368-379.

**Collins BR, Parke JL, Lachenbruch B, Hansen EM.** 2009. The effects of *Phytophthora ramorum* infection on hydraulic conductivity and tylosis formation in tanoak sapwood. *Canadian Journal of Forest Research* 39, 1766-1776.

**Czemmel S, Galarneau ER, Travadon R, McElrone AJ, Cramer GR, Baumgartner K.** 2015. Genes expressed in grapevine leaves reveal latent wood infection by the fungal pathogen *Neofusicoccum parvum*. *PloS one* 10, e0121828.

**Desprez-Loustau M-L, Marçais B, Nageleisen L-M, Piou D, Vannini A.** 2006. Interactive effects of drought and pathogens in forest trees. *Annals of Forest Science* 63, 597-612.

**Deyett E, Pouzoulet J, Yang J-I, Ashworth VE, Castro C, Roper MC, Rolshausen PE.** 2019. Assessment of Pierce's disease susceptibility in *Vitis vinifera* cultivars with different pedigrees. *Plant Pathology* 68, 1079-1087.

**De Micco V, Balzano A, Wheeler EA, Baas P.** 2016. Tyloses and gums: A review of structure, function and occurrence of vessel occlusions. *IAWA Journal* 37, 186-205.

**Elgersma DM.** 1970. Length and diameter of xylem vessels as factors in resistance of elms to *Ceratocystis ulmi*. *Netherlands Journal of Plant Pathology* 76, 179-182.

**Eskalen A, Stouthamer R, Lynch SC, Rugman-Jones PF, Twizeyimana M, Gonzalez A, Thibault T.** 2013. Host Range of *Fusarium Dieback* and Its *Ambrosia Beetle* (Coleoptera : Scolytinae) Vector in Southern California. *Plant Disease* 97, 938-951.

**Et-Touil A, Rioux D, Mathieu FM, Bernier L.** 2005. External symptoms and histopathological changes following inoculation of elms putatively resistant to Dutch elm disease with genetically close strains of *Ophiostoma*. *Canadian Journal of Botany* 83, 656-667.

**Fallon B, Yang A, Lapadat C, Armour I, Juzwik J, Montgomery RA, Cavender-Bares J.** 2020. Spectral differentiation of oak wilt from foliar fungal disease and drought is correlated with physiological changes. *Tree Physiology* 40, 377-390.

**Fradin EF, Thomma BPHJ.** 2006. Physiology and molecular aspects of *Verticillium* wilt diseases caused by *V. dahliae* and *V. albo-atrum*. *Molecular Plant Pathology* 7, 71-86.

**Gärtner H, Lucchinetti S, Schweingruber FH.** 2014. New perspectives for wood anatomical analysis in dendrosciences: the GSL1-microtome. *Dendrochronologia* 32, 47-51.

**Goberville E, Hautekèete N-C, Kirby RR, Piquot Y, Luczak C, Beaugrand G.** 2016. Climate change and the ash dieback crisis. *Scientific Reports* 6 doi:10.1038/srep35303.

**Gramaje D, Úrbez-Torres JR, Sosnowski MR.** 2018. Managing Grapevine Trunk Diseases With Respect to Etiology and Epidemiology : Current Strategies and Future Prospects. *Plant Disease* 102, 12-39.

**Guérard N, Maillard P, Bréchet C, Lieutier F, Dreyer E.** 2007. Do trees use reserve or newly assimilated carbon for their defense reactions? A <sup>13</sup>C labeling approach with young Scots pines inoculated with a bark-beetle-associated fungus (*Ophiostoma brunneo ciliatum*). *Annals of Forest Science* 64, 601-608.

**Guerin-Dubrana L, Labenne A, Labrousse JC, Bastien S, Rey P, Gegout-Petit A.** 2013. Statistical analysis of grapevine mortality associated with esca or Eutypa dieback foliar expression. *Phytopathologia Mediterranea* 52, 276-288.

**Guerin-Dubrana L, Fontaine F, Mugnai L.** 2019. Grapevine trunk disease in European and Mediterranean vineyards: Occurrence, distribution and associated disease-affecting cultural factors. *Phytopathologia Mediterranea* 58, 49-71.

**Hochberg U, Albuquerque C, Rachmilevitch S, Cochard H, David-Schwartz R, Brodersen CR, McElrone A, Windt CW.** 2016. Grapevine petioles are more sensitive to drought induced embolism than stems: Evidence from *in vivo* MRI and microcomputed tomography observations of hydraulic vulnerability segmentation: Hydraulic vulnerability segmentation in grapevine. *Plant, Cell & Environment* 39, 1886-1894.

**Hochberg U, Windt CW, Ponomarenko A, Zhang Y-J, Gersony J, Rockwell FE, Holbrook NM.** 2017. Stomatal Closure, Basal Leaf Embolism, and Shedding Protect the Hydraulic Integrity of Grape Stems. *Plant Physiology* 174, 764-775.

**Jacobi WR, MacDonald WL.** 1980. Colonization of resistant and susceptible oaks by *Ceratocystis fagacearum*. *Phytopathology* 70, 618-623.

Kaplan J, Travadon R, Cooper M, Hillis V, Lubell, Baumgartner K. 2016. Identifying economic hurdles to early adoption of preventative practices\_ The case of trunk diseases in California winegrape vineyards. *Wine Economics and Policy* 15, 127-141.

**King A, Guignot N, Zerbino P, et al.** 2016. Tomography and imaging at the PSICHE beam line of the SOLEIL synchrotron. *Review of Scientific Instruments* 87, 093704.

**Lachenbruch B, Zhao J-P.** 2019. Effects of phloem on canopy dieback, tested with manipulations and a canker pathogen in the *Corylus avellana/Anisogramma anomala* host/pathogen system. *Tree Physiology* 39, 1086-1098.

**Lecomte P, Darrietort G, Liminana J-M, Comont G, Muruamendiaraz A, Legorburu F-J, Choueiri E, Jreijiri F, El Amil R, Fermaud M.** 2012. New Insights into Esca of Grapevine: The Development of Foliar Symptoms and Their Association with Xylem Discoloration. *Plant Disease* 96, 924-934.

**Li S, Bonneu F, Chadoeuf J, Picart D, Gégout-Petit A, Guérin-Dubrana L.** 2017. Spatial and Temporal Pattern Analyses of Esca Grapevine Disease in Vineyards in France. *Phytopathology* 107, 59-69.

**Martin N, Vesentini D, Rego C, Monteiro S, Oliveira H, Ferreira RB.** 2009. *Phaeomonniella chlamydospora* infection induces changes in phenolic compounds content in *Vitis vinifera*. *Phytopathologia Mediterranea* 48, 101-116.

**Martín JA, Solla A, Ruiz-Villar M, Gil L.** 2013. Vessel length and conductivity of *Ulmus* branches : Ontogenetic changes and relation to resistance to Dutch elm disease. *Trees* 27, 1239-1248.

**McDowell N, Pockman WT, Allen CD, et al.** 2008. Mechanisms of plant survival and mortality during drought : Why do some plants survive while others succumb to drought? *New Phytologist* 178, 719-739.

**McElrone AJ, Sherald JL, Forseth IN.** 2003. Interactive effects of water stress and xylem-limited bacterial infection on the water relations of a host vine. *Journal of Experimental Botany* 54, 419-430.

**McElrone AJ, Jackson S, Habdas P.** 2008. Hydraulic disruption and passive migration by a bacterial pathogen in oak tree xylem. *Journal of Experimental Botany* 59, 2649-2657.

**McNabb HS, Heybroek HM, Macdonald WL.** 1970. Anatomical factors in resistance to Dutch elm disease. *Netherlands Journal of Plant Pathology* 76, 196-205.

**Mensah JK, Sayer MAS, Nadel RL, Matusick G, Eckhardt LG.** 2020. Physiological response of *Pinus taeda* L. trees to stem inoculation with *Leptographium terebrantis*. *Trees* 34, 869–880.

**Mirone A, Brun E, Guillard E, Tafforeau P, Kieffer J.** 2014. The PyHST2 hybrid distributed code for high speed tomographic reconstruction with iterative reconstruction and a

priori knowledge capabilities. Nuclear Instruments and Methods in Physics Research Section B: Beam Interactions with Materials and Atoms 324, 41-48.

**Morales-Cruz A, Allenbeck G, Figueroa-Balderas R, Ashworth VE, Lawrence DP, Travadon R, Smith RJ, Baumgartner K, Rolshausen PE, Cantu D.** 2018. Closed-reference metatranscriptomics enables *in planta* profiling of putative virulence activities in the grapevine trunk disease complex: Transcriptomics of pathogen communities. *Molecular Plant Pathology* 19, 490-503.

**Mugnai L, Graniti A, Surico G.** 1999. Esca (Black Measles) and Brown Wood-Streaking : Two Old and Elusive Diseases of Grapevines. *Plant Disease* 83, 404-418.

**Ouadi L, Bruez E, Bastien S, Vallance J, Lecomte P, Domec J-C, Rey P.** 2019. Ecophysiological impacts of Esca, a devastating grapevine trunk disease, on *Vitis vinifera* L. *PloS one* 14, 1-20.

**Ouellette GB, Baayen RP, Simard M, Rioux D.** 1999. Ultrastructural and cytochemical study of colonization of xylem vessel elements of susceptible and resistant *Dianthus caryophyllus* by *Fusarium oxysporum* f.sp. *Dianthi*. *Canadian Journal of Botany* 77, 644-663.

**Paganin D, Mayo SC, Gureyev TE, Miller PR, Wilkins SW.** 2002. Simultaneous phase and amplitude extraction from a single defocused image of a homogeneous object. *Journal of Microscopy* 206, 33-40.

**Pandey S, Rishi RR, Jayaraj R, Giri K, Kumar R, Pandey A, Juwantha R, Madaan S, Bhandari MS.** 2019. *Fusarium equiseti* is associated with the wilt and dieback of *Aquilaria malaccensis* in Northeast India. *Forest Pathology* 49, e12489.

**Park J-H, Juzwik J.** 2014. *Ceratocystis smalleyi* colonization of bitternut hickory and host responses in the xylem. *Forest Pathology* 44, 282-292.

**Parke JL, Oh E, Voelker S, Hansen EM, Buckles G, Lachenbruch B.** 2007. *Phytophthora ramorum* Colonizes Tanoak Xylem and Is Associated with Reduced Stem Water Transport. *Phytopathology* 97, 1558-1567.

**Pearce RB.** 1996. Antimicrobial defences in the wood of living trees. *New Phytologist* 132, 203-233.

**Pérez-Donoso AG, Lenhof JJ, Pinney K, Labavitch JM.** 2016. Vessel embolism and tyloses in early stages of Pierce's disease. *Australian Journal of Grape and Wine Research* 22, 81-86.

**Pita P, Rodríguez-Calcerrada J, Medel D, Gil L.** 2018. Further insights into the components of resistance to *Ophiostoma novo-ulmi* in *Ulmus minor*: Hydraulic conductance, stomatal sensitivity and bark dehydration. *Tree Physiology* 38, 252-262.

**Pouzoulet J, Mailhac N, Couderc C, Besson X, Daydé J, Lummerzheim M, Jacques A.** 2013. A method to detect and quantify *Phaeoconiella chlamydospora* and *Phaeoacremonium aleophilum* DNA in grapevine-wood samples. *Applied Microbiology and Biotechnology* 97, 10163-10175.

**Pouzoulet J, Scudiero E, Schiavon M, Rolshausen PE.** 2017. Xylem Vessel Diameter Affects the Compartmentalization of the Vascular Pathogen *Phaeoconiella chlamydospora* in Grapevine. *Frontiers in Plant Science* 8, 1-13.

**Pouzoulet J, Scudiero E, Schiavon M, Santiago LS, Rolshausen PE.** 2019. Modeling of xylem vessel occlusion in grapevine. *Tree Physiology* 39, 1438-1445.

**Pouzoulet J, Rolshausen PE, Charbois R, Chen J, Guillaumie S, Ollat N, Gambetta GA, Delmas CEL.** 2020. Behind the Curtain of the Compartmentalization Process : Exploring How Xylem Vessel Diameter Impacts Vascular Pathogen Resistance. *Plant, Cell & Environment* doi: 10.1111/pce.13848.

**Pratt RB, Jacobsen AL.** 2018. Identifying which conduits are moving water in woody plants: A new HRCT-based method. *Tree Physiology* 38, 1200-1212.

**Rioux D, Blais M, Nadeau-Thibodeau N, Lagacé M, DesRochers P, Klimaszewska K, Bernier L.** 2018. First Extensive Microscopic Study of Butternut Defense Mechanisms Following Inoculation with the Canker Pathogen *Ophiognomonia clavignenti-juglandacearum* Reveals Compartmentalization of Tissue Damage. *Phytopathology* 108, 1237-1252.

**Salle A, Ye H, Yart A, Lieutier F.** 2008. Seasonal water stress and the resistance of *Pinus yunnanensis* to a bark-beetle-associated fungus. *Tree Physiology* 28, 679-687.

**Salleo S, Nardini A, Lo Gullo MA, Ghirardelli LA.** 2002. Changes in stem and leaf hydraulics preceding leaf shedding in *Castanea sativa* L. *Biologia plantarum* 45, 227-234.

**Schneider CA, Rasband WS, Eliceiri KW.** 2012. NIH Image to ImageJ : 25 years of image analysis. *Nature Methods* 9, 671-675.

**Shigo AL.** 1984. Compartmentalization: A conceptual framework for understanding how trees grow and defend themselves. *Annual Review of Phytopathology*, 22, 189–214.

**Sperry JS, Donnelly JR, Tyree MT.** 1988. A method for measuring hydraulic conductivity and embolism in xylem. *Plant, Cell & Environment* 11, 35-40.

**Solla A, Gil L.** 2002. Xylem vessel diameter as a factor in resistance of *Ulmus minor* to *Ophiostoma novo-ulmi*. *Forest Pathology* 32, 123-134.

**Sun Q, Rost TL, Matthews MA.** 2008. Wound-induced vascular occlusions in *Vitis vinifera* (Vitaceae) : Tyloses in summer and gels in winter. *American Journal of Botany* 95, 1498-1505.

**Sun Q, Sun Y, Walker MA, Labavitch JM.** 2013. Vascular Occlusions in Grapevines with Pierce's Disease Make Disease Symptom Development Worse. *Plant Physiology* 161, 1529-1541.

**Surico G, Marchi G, Ferrandino A, Braccini P, Mugnai L.** 2000. Analysis of the spatial spread of esca in some Tuscan vineyards (Italy). *Phytopathologia Mediterranea* 39, 211-224.

**Talboys PW.** 1972. Resistance to Vascular Wilt Fungi. *Proceedings of the Royal Society of London. Series B, Biological Science* 181, 319-332.

**Torres-Ruiz JM, Sperry JS, Fernández JE.** 2012. Improving xylem hydraulic conductivity measurements by correcting the error caused by passive water uptake. *Physiologia Plantarum* 146, 129-135.

**Travadon R, Lecomte P, Diarra B, Lawrence DP, Renault D, Ojeda H, Rey P, Baumgartner K.** 2016. Grapevine pruning systems and cultivars influence the diversity of wood-colonizing fungi. *Fungal Ecology* 24 82-93.

**Tyree MT, Sperry JS.** 1989. Vulnerability of Xylem to Cavitation and Embolism. *Annual Review of Plant Physiology and Plant Molecular Biology* 40, 19-38.

**Tyree MT, Ewers FW.** 1991. The hydraulic architecture of trees and other woody plants. *New Phytologist* 119, 345-360.

**Úrbez-Torres JR, Peduto F, Vossen PM, Krueger WH, Gubler WD.** 2013. Olive Twig and Branch Dieback: Etiology, Incidence, and Distribution in California. *Plant Disease* 97, 231-244.

**Venturas M, López R, Martín JA, Gascó A, Gil L.** 2014. Heritability of *Ulmus minor* resistance to Dutch elm disease and its relationship to vessel size, but not to xylem vulnerability to drought. *Plant Pathology* 63, 500-509.

**Yadeta KA, Thomma BPHJ.** 2013. The xylem as battleground for plant hosts and vascular wilt pathogens. *Frontiers in Plant Science* 4 doi:10.3389/fpls.2013.00097.

**Yazaki K, Takanashi T, Kanzaki N, Komatsu M, Levia DF, Kabeya D, Tobita H, Kitao M, Ishida A.** 2018. Pine wilt disease causes cavitation around the resin canals and irrecoverable xylem conduit dysfunction. *Journal of Experimental Botany* 69, 589-602.

**Zimmermann MH.** 1979. The Discovery of Tylose Formation by a Viennese lady in 1845. *IAWA Bulletin* 2, 51-56.



## TABLES

**Table 1.** Esca leaf symptom observations over the experimental season on *Vitis vinifera* cv Sauvignon blanc.

<b>Symptom notation before 2019</b>	<b>All plants</b>	<b>Previously asymptomatic (pA)</b>	<b>Previously symptomatic (pS)</b>
<b>Symptom notation in 2019</b>			
Esca-symptomatic	35 % (20/58)	30 % (6/20)	37 % (14/38)
Control-asymptomatic	65 % (38/58)	70 % (14/20)	63 % (24/38)

Plants are grouped by their symptom history: previously asymptomatic (pA, plants that have never expressed leaf symptoms between 2012 and 2018) and previously symptomatic (pS, plants that have expressed leaf symptoms at least once since 2012). Ratios present the number of plants in each symptom category (esca-symptomatic or control-asymptomatic) over the total number of plants of the category.

**Table 2.** Values for specific stem hydraulic conductivity ( $k_s$ ), theoretical stem hydraulic conductivity ( $k_{th}$ ) and equations of regression lines between  $k_s$  and  $k_{th}$  for control and esca symptomatic stems.

Tyloses	Esca	$k_s$ [kg s <sup>-1</sup> m <sup>-1</sup> MPa <sup>-1</sup> ]	$k_{th}$ [kg s <sup>-1</sup> m <sup>-1</sup> MPa <sup>-1</sup> ]	n (stem - plant)	Regression
	Control	24.97 ± 1.72	78.36 ± 4.51	39 - 23	$k_s = 0.3 \times k_{th} + 1.6$ R <sup>2</sup> =0.61 P<0.0001
Absence	Asymptomatic before symptoms	26.04 ± 4.71	74.75 ± 11.80	6 - 6	$k_s = 0.36 \times k_{th} - 0.94$ R <sup>2</sup> =0.82 P=0.013
	Pre-symptomatic	30.32 ± 4.26	87.88 ± 8.54	11 - 7	$k_s = 0.37 \times k_{th} - 1.9$ R <sup>2</sup> =0.54 P=0.010
	Asymptomatic after symptoms	19.80 ± 5.18	72.58 ± 12.64	5 - 2	$k_s = 0.33 \times k_{th} - 4$ R <sup>2</sup> =0.64 P=0.104
	Esca (tiger-stripe)	21.29 ± 5.40	72.85 ± 10.41	9 - 5	$k_s = 0.45 \times k_{th} - 11.26$ R <sup>2</sup> =0.74 P=0.003
	Esca (tiger-stripe)	11.27 ± 2.86	70.44 ± 7.81	15 - 5	$k_s = 0.17 \times k_{th} - 0.84$ R <sup>2</sup> =0.22 P=0.077
Presence	Esca (apoplectic)	2.47 ± 1.45	74.80 ± 33.48	3 - 2	$k_s = 0.04 \times k_{th} - 0.2$ R <sup>2</sup> =0.68 P=0.385
Absence	All	25.06 ± 1.46	78.42 ± 3.37	70 - 37	$k_s = 0.34 \times k_{th} - 1.90$ R <sup>2</sup> =0.63 P<0.0001
Presence	All	9.81 ± 2.51	71.16 ± 8.00	18 - 7	$k_s = 0.12 \times k_{th} - 1.28$ R <sup>2</sup> =0.15 P=0.117

Values represent mean ± SE. n = sample size, (including the number of analyzed stems and-number of analyzed plants, respectively). See text and Fig. 4 for statistical analysis. A detailed esca symptom notation is provided in Fig. 1A. Bivariate plots of each regression are presented in Fig. S4.

**Table 3.** Long-term impact of symptom presence (i.e. comparing plants with different disease history record) in control plants on specific stem hydraulic conductivity ( $k_s$ ), theoretical stem hydraulic conductivity ( $k_{th}$ ), stem total vessel density, and amount of *Phaeomonniella chlamydospora* and *Phaeoacremonium minimum* DNA in trunks of plants without foliar symptoms.

	Previously asymptomatic (pA)	Previously asymptomatic (pS)	Type III Tests of Fixed Effects (pA vs pS)
$k_s$ [kg s <sup>-1</sup> m <sup>-1</sup> MPa <sup>-1</sup> ]	23.76 ± 2.30	26.54 ± 2.61	n=39, F <sub>1,16</sub> =1.19, P=0.29
$k_{th}$ [kg s <sup>-1</sup> m <sup>-1</sup> MPa <sup>-1</sup> ]	72.22 ± 4.85	86.30 ± 7.98	n=39, F <sub>1,16</sub> =3.01, P=0.10
total vessel density [count mm <sup>-2</sup> ]	57.28 ± 4.03	52.61 ± 3.25	n=39, F <sub>1,16</sub> =0.72, P=0.41
<i>P. chlamydospora</i> [pg ng <sup>-1</sup> ]	6.14 ± 1.90	10.15 ± 3.41	<b>n=13, F<sub>1,11</sub>=5900.06, P&lt;0.0001</b>
<i>P. minimum</i> [pg ng <sup>-1</sup> ]	9.27 ± 6.97	26.40 ± 13.83	<b>n=13, F<sub>1,11</sub>=51014, P&lt;0.0001</b>

Values represent means ± SE. Pathogen quantification was estimated as: pg fungal DNA ng<sup>-1</sup> total DNA. Statistical tests used are individual generalized linear mixed models to compare pA vs pS plants (fixed effect) with the individual plants entered as a random effect in the models and the year of uprooting as a co-variable (fixed effect). Statistically significant results (P<0.05) are shown in bold.

**Table 4.** Quantification by qPCR of *Phaeomoniella chlamydospora* and *Phaeoacremonium minimum* DNA in stems and trunks of different esca symptomatology.

Organ	Esca	n	<i>P. chlamydospora</i> [pg ng <sup>-1</sup> ]	<i>P. minimum</i> [pg ng <sup>-1</sup> ]
Stem	Control	8	0	0
	Pre-symptomatic	3	0	0
	Asymptomatic (after symptoms)	3	0	0
	Tiger-stripe (without tyloses)	4	0	0
	Tiger-stripe (with tyloses)	8	0	0
	Apoplectic	2	0	0
Trunk	Control	13	7.37 ± 1.67 (12/13)*	14.54 ± 6.51 (12/13)*
	Symptomatic	7	15.80 ± 3.12 (7/7)*	23.90 ± 8.82 (7/7)*

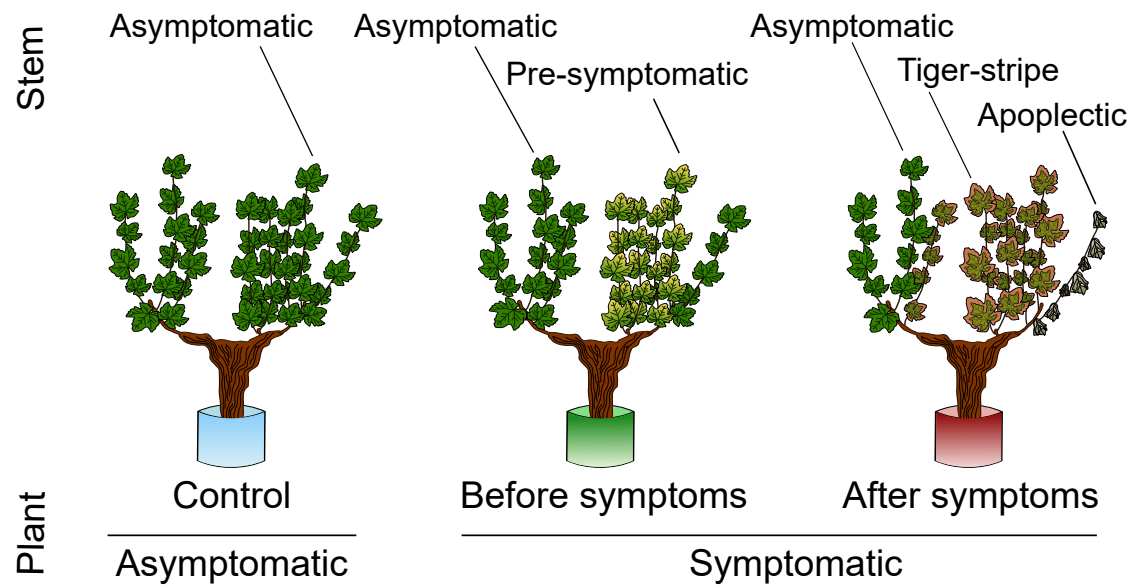
\*Number of samples positive for the pathogen over the total number of analyzed samples.

Pathogen quantification was estimated as: pg fungal DNA per ng total DNA. Values represent means ± SE, n = sample size. Trunks of symptomatic plants presented higher amount of both *P. chlamydospora* and *P. minimum*, compared to control (n=20, F<sub>1,18</sub>=29806.11.25, P<0.0001 and n=20, F<sub>1,18</sub>=21925.4, P<0.0001, respectively). See text for statistical methods.

## FIGURES

**A**

Esca symptom notation



**B**

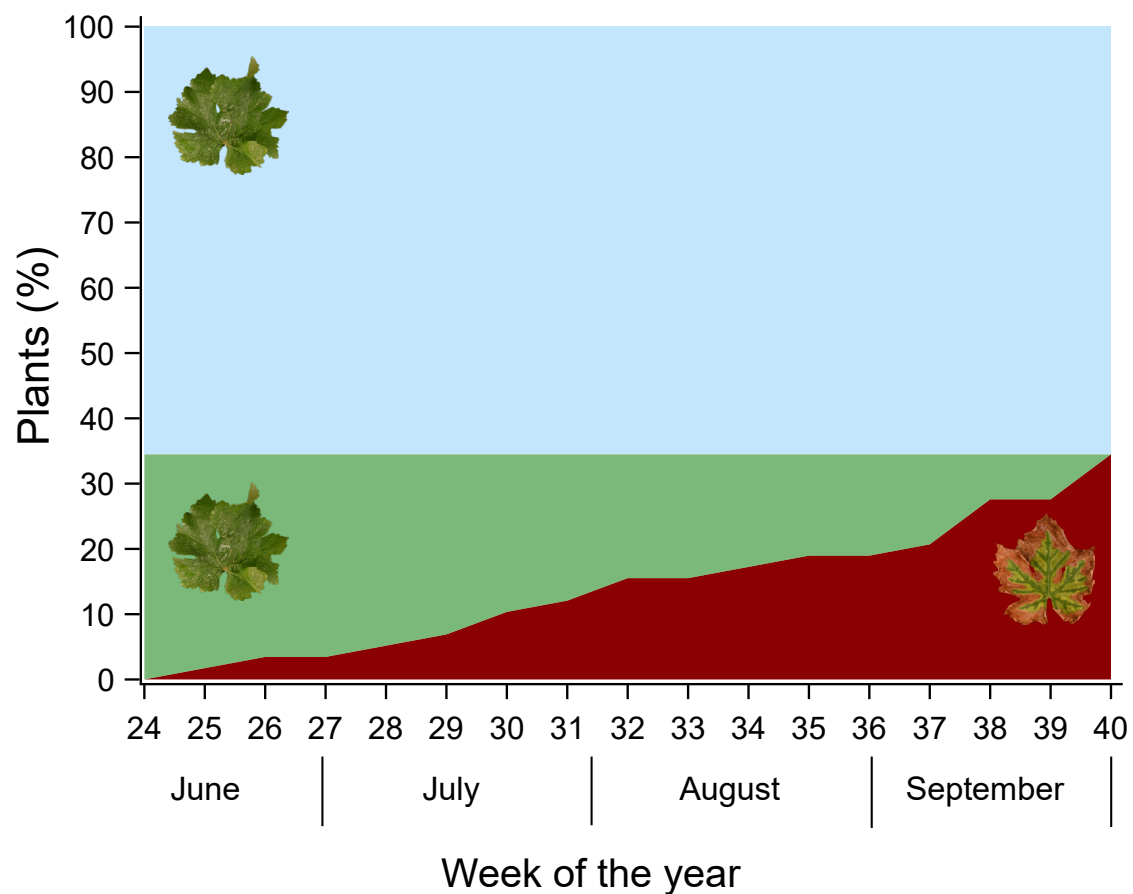


**Fig. 1.** Representation of esca symptom notation during the experimental season. (A) Single stems could be noted as esca asymptomatic, pre-symptomatic, tiger-stripe, or apoplectic. Whole plants have been noted as control (asymptomatic from June to October) or symptomatic (with tiger-stripe symptoms at the end of the season). (B) Proportion of plants in each symptom category over the experimental season (n=58). The blue area corresponds to control plants, green area to esca symptomatic plants before symptom appearance, and red area to esca symptomatic plants.

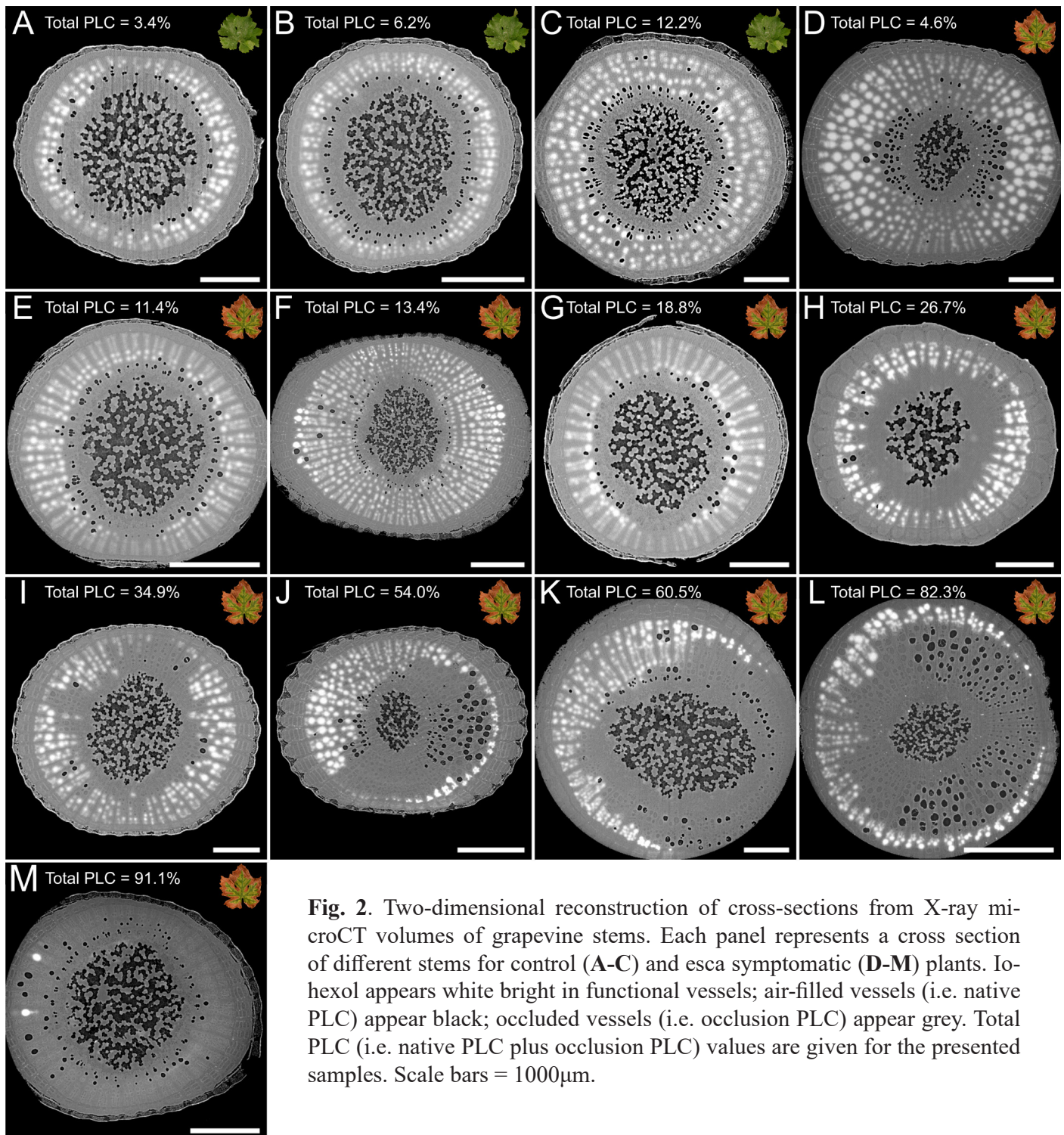


**Fig. 2.** Two-dimensional reconstruction of cross-sections from X-ray microCT volumes of grapevine stems. Each panel represents a cross section of different stems for control (A-C) and esca symptomatic (D-M) plants. Iohexol appears white bright in functional vessels; air-filled vessels (i.e. native PLC) appear black; occluded vessels (i.e. occlusion PLC) appear grey. Total PLC (i.e. native PLC plus occlusion PLC) values are given for the presented samples. Scale bars = 1000 $\mu$ m.

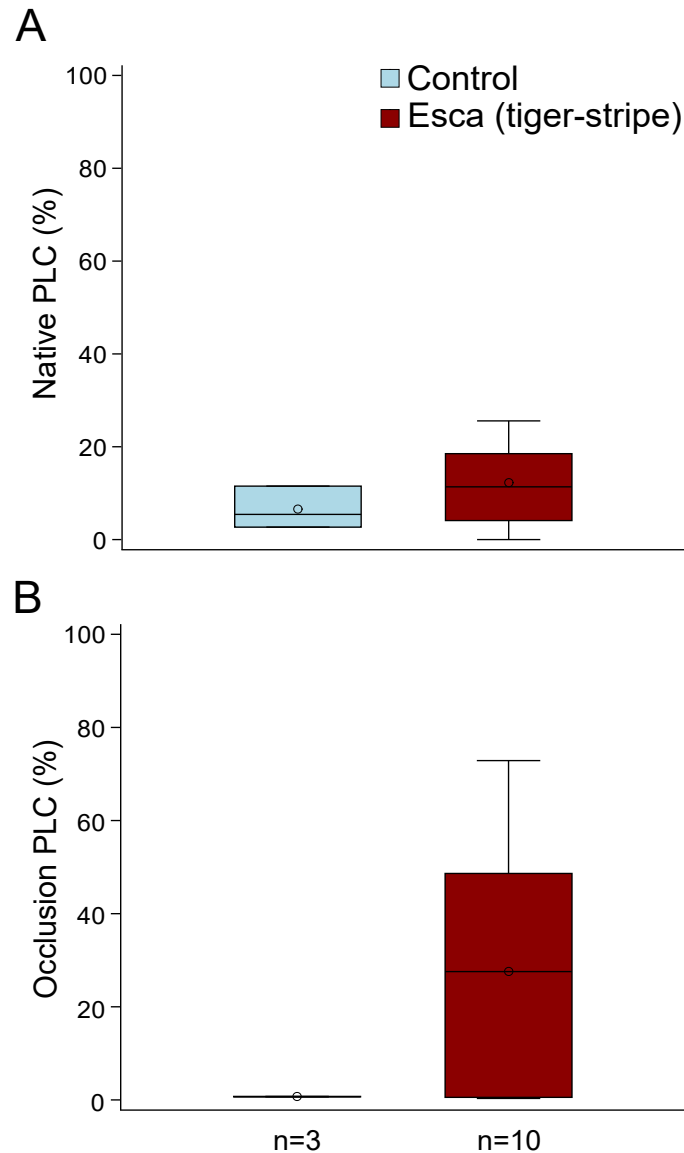


**Fig. 3.** (A) Mean values of native PLC in control (blue) and esca tiger-stripe (red) stems of grapevine plants using X-ray microCT imaging. Differences were not significant ( $n=13$ ,  $F_{1,9}=0.07$ ,  $P=0.79$ ). (B) Mean values of occlusion PLC in control (blue) and esca tiger-stripe (red) stems of grapevine plants using X-ray microCT imaging. Differences were not significant ( $n=13$ ,  $F_{1,9}=0.33$ ,  $P=0.58$ ). Boxes and bars show the median, quartiles and extreme values, circles show mean values. N represents the sample size (number of analyzed stems) for each group.



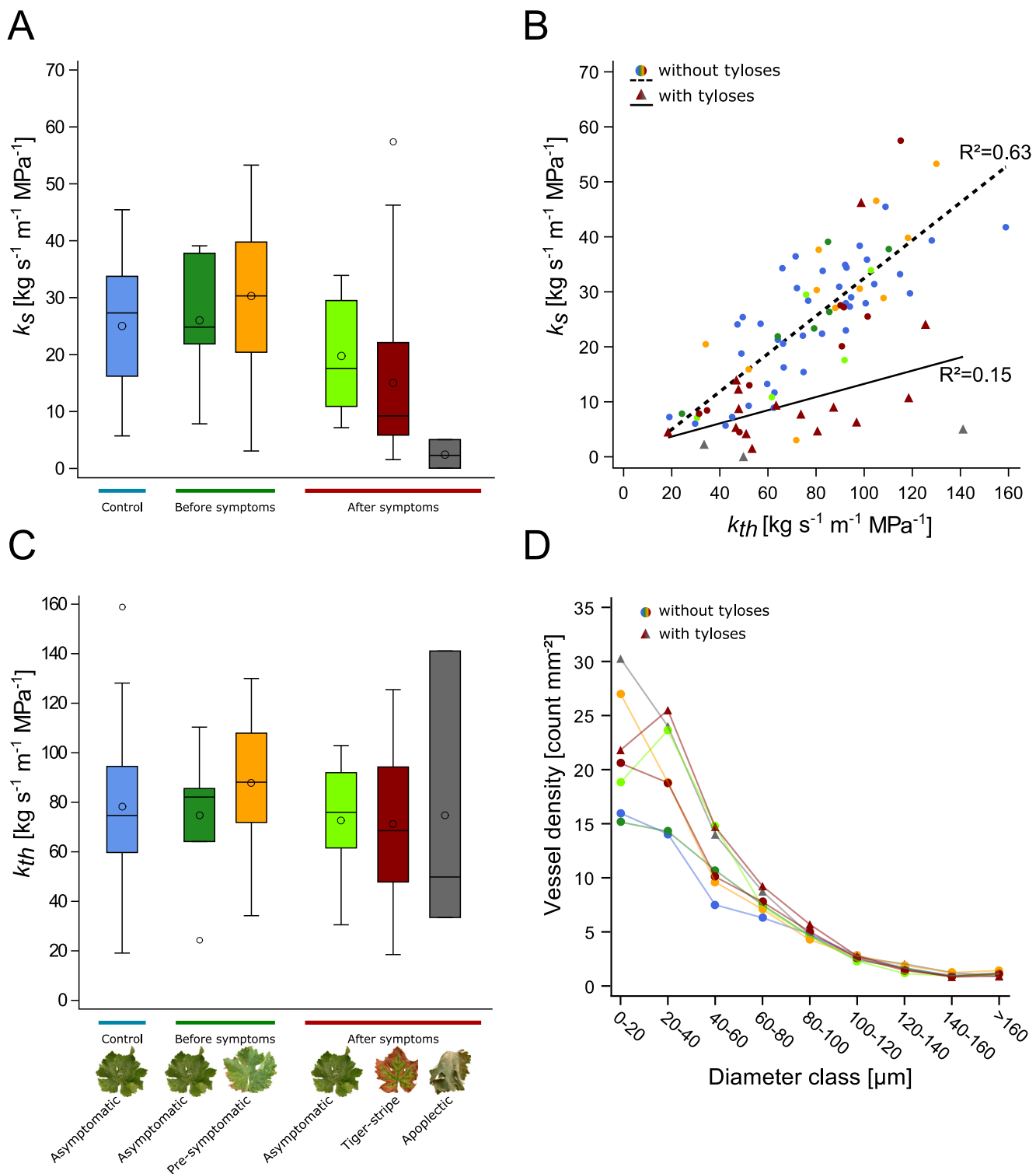


**Fig. 4.** Relationships between specific stem hydraulic conductivity ( $k_s$ ), theoretical stem hydraulic conductivity ( $k_{th}$ ), and vessel density in control and esca symptomatic grapevine plants. **(A)**  $k_s$  values for control (blue); asymptomatic (dark green) and pre-symptomatic (yellow) stems in plants before symptom appearance; asymptomatic (light green), tiger-stripe (red), and apoplectic (grey) stems in plants after symptom appearance, differences were not significant ( $n=88$ ,  $F_{5,45}=1.30$ ,  $P=0.28$ ). Boxes and bars show the median, quartiles and extreme values, circles within boxes correspond to means, and circles outside boxes to outlier values. **(B)** Relationships between  $k_s$  and  $k_{th}$ . Symbols represent the absence (circles) or presence (triangles) of tyloses in xylem vessels. Colors represent esca symptomatology (as in panel A). The dashed line represents the regression for stems in which no tyloses were observed in xylem vessels, and the solid line represents the regression for samples with tyloses.  $R^2$  for the regression lines are indicated (see Table 2 and Fig. S4 for detailed analyses). **(C)**  $k_{th}$  values for the different stem categories as presented in panel a. Differences were not significant ( $n=88$ ,  $F_{5,45}=0.58$ ,  $P=0.71$ ). **(D)** Relationships between mean values of xylem vessel density and their diameters. Differences in total vessel density and in vessel size distributions were not significant ( $n=88$ ,  $F_{6,45}=0.77$ ,  $P=0.60$ ;  $n=792$  (88 samples for 9 vessel classes),  $F_{48,693}=1.19$ ,  $P=0.18$ ). Colors and markers are the same as panel B.